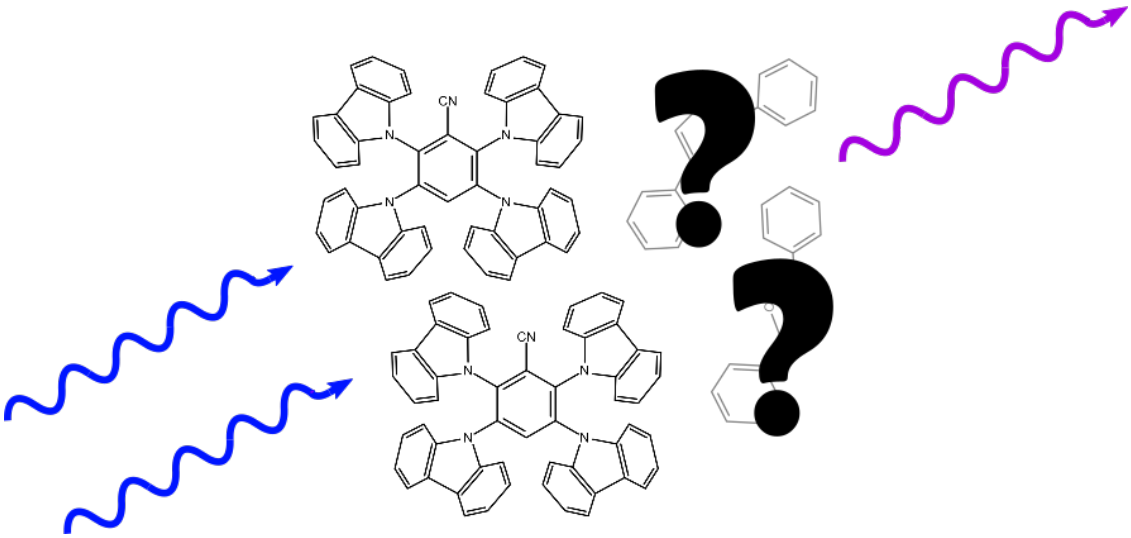
CHALMERS
UNIVERSITY OF TECHNOLOGY




# Towards more efficient visible-to-UV photon upconversion

## A study of UV emitters and their impact on the efficiency of triplet-triplet annihilation upconversion systems

Master's thesis in Nanotechnology

JESSICA JOHNSSON

DEPARTMENT OF CHEMISTRY AND CHEMICAL ENGINEERING

CHALMERS UNIVERSITY OF TECHNOLOGY
Gothenburg, Sweden 2022
www.chalmers.se

Master's thesis 2022

# Towards more efficient visible-to-UV photon upconversion

A study of UV emitters and their impact on the efficiency of triplet-triplet annihilation upconversion systems

JESSICA JOHNSSON




CHALMERS
UNIVERSITY OF TECHNOLOGY

Department of Chemistry and Chemical Engineering
*Division of Chemistry and Biochemistry*
Albinsson Research Group
Chalmers University of Technology
Gothenburg, Sweden 2022

Towards more efficient visible-to-UV photon upconversion
A study of UV emitters and their impact on the efficiency of triplet-triplet annihilation upconversion systems
JESSICA JOHNSSON

© JESSICA JOHNSSON, 2022.

Supervisor: Axel Olesund, Department of Chemistry and Chemical Engineering
Examiner: Bo Albinsson, Department of Chemistry and Chemical Engineering

Master's Thesis 2022
Department of Chemistry and Chemical Engineering
Division of Chemistry and Biochemistry
Albinsson Research Group
Chalmers University of Technology
SE-412 96 Gothenburg
Telephone +46 31 772 1000

Cover: Illustration of photon upconversion from blue visible light to ultraviolet light, with two sensitizer molecules (2,3,5,6-tetra(9H-carbazol-9-yl)benzonitrile) and two undefined annihilator molecules.

Typeset in LaTeX
Gothenburg, Sweden 2022

Towards more efficient visible-to-UV photon upconversion
A study of UV emitters and their impact on the efficiency of triplet-triplet annihilation upconversion systems
JESSICA JOHNSSON
Department of Chemistry and Chemical Engineering
Chalmers University of Technology

# Abstract

It is generally acknowledged that the usage of fossil fuels has several negative environmental impacts, and for its ongoing replacement, the sun is one of the most promising energy sources. The sunlight consists of photons with a broad spectrum of energies, but due to the mismatch with the solar energy device, only a fraction of the photons can be harvested by today's devices. The efficiency of solar energy harvesting can therefore be increased by exploiting a wider range of the solar spectra.

Photon upconversion (UC) is a technique which converts low-energy light to light of higher energy. In this thesis, upconversion from visible to ultraviolet (vis-to-UV) has been studied. Vis-to-UV upconversion is especially interesting due to the importance of UV-light for some photochemical reactions, for example producing hydrogen gas through water splitting, and the scarcity of UV-light compared to the abundant visible sunlight.

Here, the photon upconversion has been realized through a process called triplet-triplet annihilation, which utilizes two different compounds, called sensitizer and annihilator. The sensitizer is responsible for light absorption, and in this study, a compound which exhibit thermally activated delayed fluorescence was used, namely, the purely organic compound 2,3,5,6-tetra(9H-carbazol-9-yl)benzonitrile (4CzBN). The annihilator emits the upconverted photons, and six different UV emitting molecules have been studied in this project.

Four of the UV emitters have been used as annihilators previously, some which have achieved high efficiencies, and some relatively low, while two compounds were new in this application. The aim of the project was to increase the knowledge about annihilators and their impact on the UC efficiency, and therefore, several characteristics important for the UC process were evaluated, in addition to the overall UC efficiency.

Upconverted emission were observed from all six annihilators when paired with the sensitizer 4CzBN, and with excellent efficiencies compared to previous studies. Unfortunately, the UC emission was very unstable and degraded over time, however, the results indicate that the solvent largely affects the system stability. From the measured UC characteristics, it was concluded that the annihilator triplet excited state lifetime was the most important parameter affecting the overall UC efficiency.

Keywords: upconversion, visible-to-UV, efficiency, annihilator, UV emitter, triplet-triplet annihilation, spectroscopy.

# Acknowledgements

To begin with, I would like to thank my supervisor Axel Olesund, who not only suggested the project and adeptly guided me through it but did so with a lot of enthusiasm and kindness. I would also like to thank my examiner Bo Albinsson, for encouraging me to get in touch about Master's thesis projects during the spectroscopy course, since it lead me to this very exciting subject that is photon upconversion. In addition, I would like to give a special thank you to both Axel and Bo for showing such compassion, understanding and patience regarding my mental health issues and its consequent obstacles, for which I am very grateful.

I would like to thank Fredrik Edhborg for showing me around the lab in the beginning of the project, and for thoroughly answering questions, often leaving me with new questions or ideas. I would also like to thank Rasmus, Wera, Deise, and Lili for helping me around the lab whenever I needed. Moreover, thank you everyone in the spectroscopy group, I may not have gone to all group meetings, but when I did, it was always instructive and interesting.

I would also like to thank all the people who have made my years at Chalmers enjoyable and gratifying. Last but not least, I want to thank my family for all their support and for believing in me, especially Oscar, who I'm not sure I could have done this without.

Jessica Johnsson, Gothenburg, July 2022

# Contents

**List of Figures** **xi**

**List of Tables** **xiii**

**1 Introduction** **1**
1.1 Purpose . . . 2
1.2 Scope . . . 2

**2 Theory** **3**
2.1 Light and matter . . . 3
2.1.1 Electrons and electronic states . . . 3
2.1.2 Decay processes . . . 5
2.1.3 Some useful concepts . . . 6
2.2 Photon upconversion . . . 7
2.2.1 Dexter energy transfer . . . 7
2.2.2 Triplet-triplet annihilation . . . 8
2.2.3 Upconversion efficiency . . . 9
2.2.3.1 Spin statistical factor . . . 9
2.2.3.2 Excitation intensity . . . 10
2.3 TADF sensitizer . . . 11
2.3.1 TET rate and efficiency for TADF sensitizers . . . 13
2.4 Annihilators . . . 14

**3 Methods** **17**
3.1 Steady-state absorption spectroscopy . . . 17
3.2 Steady-state emission spectroscopy . . . 18
3.2.1 Upconversion measurements . . . 19
3.3 Time-resolved emission spectroscopy . . . 19
3.4 Calculations and fitting procedures . . . 20
3.4.1 Quantum yields . . . 20
3.4.2 Upconversion quantum yields . . . 20
3.4.3 Intensity threshold . . . 21
3.4.4 Annihilator triplet lifetimes . . . 22

**4 Results & Discussion** **25**
4.1 Sensitizer photophysical characterisation . . . 25
4.2 Annihilator photophysical characterization . . . 26

4.3 Upconversion measurements . . . . . 28
4.3.1 TET rates and efficiencies . . . . . 28
4.3.2 Triplet lifetimes . . . . . 29
4.3.3 $\beta$ values and TTA efficiency . . . . . 29
4.3.4 Intensity thresholds . . . . . 30
4.3.5 Upconversion quantum yields . . . . . 31
4.3.5.1 System instability and solvents . . . . . 32
4.3.5.2 Scattering and 2PI solubility . . . . . 33

**5 Conclusion** **35**

**Bibliography** **37**

**A Appendix 1: Derivations** **I**
A.1 TET efficiency for TADF sensitizers . . . . . I
A.2 Determination of TET rate . . . . . II

**B Appendix 2: Additional figures** **III**

# List of Figures


2.1 Schematics of electron spin in a two-electron system. . . . . 5
2.2 Jablonski diagram. Thick horizontal lines represent electronic energy levels, $S_i$ and $T_i$ denotes singlet and triplet energy levels. Thin horizontal lines correspond to vibrational levels. Vibrational relaxation (VR) is depicted by vertical, dotted arrows, internal conversion (IC) and intersystem crossing (ISC) by dashed, horizontal arrows. Colored, vertical arrows represent events involving the absorption or emission of a photon. . . . . 5
2.3 The process of sTTA-UC. Firstly, the sensitizers are excited by the absorption of a photon. They then experience ISC creating triplet excited sensitizers. The excitations are transferred to the annihilators by TET. Two annihilators interact through TTA, creating a singlet excited annihilator. At last, the annihilator emits a photon with higher energy then the photons originally absorbed by the sensitizers. 8
2.4 Jablonski diagram depicting the different decay processes for a TADF compound alongside the process of sTTA-UC using a TADF compound as sensitizer. . . . . 12
2.5 The molecular structure of the sensitizer 4CzBN. . . . . 12
2.6 The molecular structures, full names and acronyms of the annihilators. 14

3.1 Schematic illustration of the experimental setup for absorption measurements. . . . . 17
3.2 Schematic illustration of the experimental setup for emission measurements. . . . . 18
3.3 An example showing the fittings of the UC emission spectra used to calculate $\Phi_{UC,g}$ and $\Phi_{UC}$. . . . . 21
3.4 Illustrative example of excitation intensity dependence of UC emission intensity in a double logarithmic plot and a methodology to obtain the intensity threshold ($I_{th}$). The red and blue shaded areas indicate the regions of quadratic and linear excitation intensity dependence, respectively. . . . . 22

4.1 Normalized absorption (solid), fluorescence (dashed) and phosphorescence (dotted pink) spectra of the sensitizer 4CzBN. . . . . 25
4.2 Normalized absorption (solid) and emission (dashed) spectra of the annihilators measured at room temperature in THF. . . . . 27

4.3 Stern-Volmer plots showing the change of 4CzBN delayed component lifetime upon addition of different concentrations of annihilator. . . . 28
4.4 Determination of PPO triplet lifetime. Normalized time-domain measurement of UC emission from 100 $\mu$M 4CzBN / 10 mM PPO at different excitation intensities, globally fitted according to Equation 3.5. . . . 30
4.5 Determination of intensity threshold for TIPS-naph. . . . 30
4.6 Quantum yields of UC photons generated (solid) and UC photons observed (striped). The error bars indicate the standard deviation. . . 31
4.7 The decrease of UC emission intensity over time for samples of 25 $\mu$M 4CzBN and 10mM PPF (red lines) or TP (purple lines) in (A) THF, and (B) toluene. . . . 33
4.8 (A) Absorption spectra of 4CzBN (dashed line), and 4CzBN + 10 mM 2PI measured before (green) and after (brown) 80 minutes of 405 nm laser irradiation. (B) Time development of UC emission signal for 2PI measured at 356 nm. . . . 34

B.1 Determination of PPD, TP and TIPS-naph triplet lifetimes. Global fitting of UC emission from 100 $\mu$M 4CzBN / 10 mM annihilator according to Equation 3.5. . . . III
B.2 Determination of 2PI and PPF triplet lifetimes. Global fitting of UC emission from 100 $\mu$M 4CzBN / 1 mM annihilator according to Equation 3.5. . . . IV
B.3 Measured UC spectra (black) and fitted spectra to calculate $\Phi_{UC,g}$ (blue) and $\Phi_{UC,g}$ (red) for the different annihilators. . . . V
B.4 Examples of how the UC emission intensity decrease over time. . . . VI

# List of Tables

2.1 Triplet excited state energies from literature. . . . . 15

4.1 Photophysical characteristics of the sensitizer 4CzBN. . . . . 26
4.2 Photophysical characteristics of the annihilators. . . . . 26
4.3 Measured values of UC quantum yields and parameters important for TTA-UC systems. . . . . 28

# 1
# Introduction

Society is vitally dependent on energy and has been for hundreds of years. Fossil fuels have been the main energy source for a long time, but in these days, it is generally acknowledged that its usage have several negative environmental impacts, such as global warming and air pollution. To fulfil the energy demand without continuing damaging the planet we must use other energy sources, of which one of the most promising is the sun.[1] Nevertheless, the use of solar energy is not without challenges. Solar technologies are facing several barriers, both technical, as low solar cell efficiencies, and others, such as economic hindrances.

There are many factors that affect the efficiency of solar cells, the absorption spectrum is one of them. Solar cells can only absorb photons from a limited region of light, depending on the material of which the cells are constructed. Expanding the absorbing region could therefore be one way to increase solar cell efficiencies.[2] However, an alternative way to enhance light harvesting is to transform the incoming photons by up- or down-conversion.[3]

Photon upconversion (UC) is a process in which low-energy light of long wavelengths is converted to light of higher energy, and by using various system combinations, UC can be achieved in several different parts of the light spectrum.[4] Recently, a composition has been reported that is capable of upconverting near-infrared light from below the silicon bandgap, which is noteworthy since it is a requirement for applications of UC with silicon solar cells.[5] Another way of using UC is to start with visible light and transform it to ultraviolet (UV) light. Upconversion from visible to ultraviolet (vis-to-UV) is particularly interesting due to the importance of UV-light for some photochemical reactions,[6] and from the scarcity of UV-light compared to the abundant visible sunlight. A long-term ambition is to be able to utilize upconverted sunlight to produce hydrogen gas through water-splitting, a photochemical reaction where water is divided into hydrogen and oxygen gas. Hydrogen gas is considered a future transportation fuel due to its environmentally friendly oxidation product, namely water.[7] Producing hydrogen gas through water splitting has great potential as a quantum yield of 56 % have been shown when utilizing 270 nm light.[8] However, to realize water splitting using sunlight, one prerequisite is to first improve the efficiency of vis-to-UV upconversion.

One way to implement UC to the UV-region from low power visible light is to utilize a process called sensitized triplet-triplet annihilation (TTA).[9] The process combines the energy from two low-energy photons into one photon of higher energy, and involves energy transfer from a donor molecule, called sensitizer, to an acceptor molecule, called annihilator. When combining molecules to a viable UC system there are several requirements for the sensitizer and annihilator molecules, where

one of the more basic conditions is the ability to absorb and emit light from suitable parts of the spectrum. This of course implies that to achieve vis-to-UV UC, the sensitizer must effectively absorb visible light, and the annihilator must emit in the UV region.

The first TTA-based vis-to-UV photon upconversion was presented in 2009 and had a quantum yield of 0.58 %,[9] while today, quantum yields just above 10 % have been recorded.[10, 11, 12] Note that the quantum yields should be compared to the upper theoretical value of 50 % since the process includes a transformation of two photons into one photon. Although a clear progress has been made, the efficiency for UC to the UV-region is still relatively low compared to UC in other parts of the solar spectrum, where quantum yields as high as 42 % have been reported.[13] The reasons why it is harder to achieve effective vis-to-UV UC is partly unknown. One possible contributor is that relatively few annihilator molecules have been reported that upconverts to the UV-region, and their UC characteristics are largely uncharted. Deeper knowledge about the properties of UV emissive annihilators may in the future facilitate the discovery of new and more effective vis-to-UV UC systems.

## 1.1 Purpose

The purpose of this project is to examine and compare annihilators used for upconversion to the UV-region. The efficiency for systems with the different molecules will be evaluated, and measurements will be conducted to determine lifetimes, rate constants, quantum yields etc., relevant for the upconversion process. The aim is that this project will contribute to increased understanding for why some annihilator molecules give higher efficiencies than others.

## 1.2 Scope

This project will examine and compare annihilators in a TTA-based upconversion (TTA-UC) system, and the studied annihilators are limited to six molecules. The aim is to understand why some annihilators are more efficient than others, not to attain new record high quantum yields. Therefore, the annihilators are chosen to be a range of molecules, some known to achieve high efficiencies, and some relatively low. Furthermore, two new candidates will also be studied.

The sensitizer is vital for the TTA-UC process, and the choice of sensitizer can have a large impact on the overall efficiency of the system. However, the focus of this project is neither the sensitizer nor the efficiency. Thus, for easier comparison of the annihilators, only one sensitizer will be used within this project.

# 2
# Theory

## 2.1 Light and matter

In classical physics, light can be described as a harmonic wave of two oscillating fields, one electric and one magnetic. All light has a frequency ($\nu$) and a wavelength ($\lambda$). The wavelength is defined as the distance over which the shape of the wave repeats, which for harmonic waves is the distance between two maxima. The wavelengths of visible light range from about 400 to 700 nm. Light with shorter wavelengths is known as ultraviolet (UV) light and has wavelengths down to 10 nm, while infrared (IR) light has longer wavelengths, up to 1 mm.

From quantum mechanical insights it is known that light can also be described as a flow of discrete particles called photons. The two natures, or descriptions, of light is called the *wave-particle duality*. The energy ($E$) of a single photon can easily be calculated from its frequency and *Planck's constant* ($h = 6.626 \times 10^{-34}$ Js),

$$E = h\nu = \frac{hc}{\lambda} \tag{2.1}$$

or alternatively, using the wavelength and the speed of light ($c = 2.998 \times 10^8$ m/s). Equation 2.1 show that the energy of light depends on the frequency or wavelength of the electromagnetic wave. Shorter wavelength equal higher energy, and thus, UV light has higher energy than visible light.

### 2.1.1 Electrons and electronic states

Interactions between light and matter are the basis for photophysics and photochemistry. While the wave-particle duality is essential for the understanding of light, knowledge about electrons and *electronic states* are necessary in order to understand light-matter interactions.

When electrons are part of an atom or a molecule, they have discrete energy levels. The electrons can therefore only exist in the electronic states that corresponds to those energy levels. When the electrons in an atom or molecule are distributed in a way so that all electrons are occupying electronic states with as low energy as possible, the compound is said to be in its ground state. When light interacts with matter it can result in absorption, scattering or if no interaction takes place, transmission. When absorption occurs, an atom or molecule receives the energy of the absorbed photon. The absorbed energy moves an electron to a state of higher energy. The total energy of the molecule has therefore increased, and the molecule is said to be in an excited state. The difference between the ground state energy

($E_{ground}$) and the energy of the excited state ($E_{excited}$) is the same as the energy of the absorbed photon,

$$\Delta E = E_{excited} - E_{ground} = h\nu \tag{2.2}$$

Electrons are fermions, which are particles with half-integer spin, or with the intrinsic angular momentum $s = \pm 1/2$. The spin magnetic quantum number, $m_s$, can therefore be either $+1/2$ or $-1/2$. However, this is more commonly referred to as spin up and spin down. The *Pauli exclusion principle* states that two or more fermions cannot occupy the same quantum state. All fermions must each have a unique set of quantum numbers. Thus, up to two electrons can occupy the same electronic orbital, one electron with spin up and one with spin down.

A useful example is a two-electron system. If the two electrons have different spin, they may occupy the same electronic orbital. If this is at the lowest energy level, the system is said to be in its ground state. If the two-electron system is in an excited state, one of the electrons has moved to an orbital of higher energy. There are then two possible ways for the excited electron to arrange, either having the same spin or opposite spin as the ground state electron. The net spin is described by the total spin angular momentum, $S$, which can take the values of

$$S = s_1 + s_2, s_1 + s_2 - 1, ..., |s_1 - s_2| \tag{2.3}$$

where $s_i$ is the intrinsic angular momentum of particle $i$. The net spin can be visualized as the coupled spin states' magnitude. For the two-electron system $S$ has two possible results, $S = 0$ and $S = 1$. The total spin magnetic quantum number, $M_S$, defines the direction of the net spin and takes the values of

$$M_S = S, S - 1, ..., -S \tag{2.4}$$

If the two electrons have antiparallel spin, that is if $s_i$ have different signs, $S = 0$ and thus, $M_S$ have only one possible value. This is called a *singlet* state. If the electrons have parallel spin, $S = 1$ and there are three possible outcomes for $M_S$, $1, 0$ and $-1$. These are called *triplet* states. The three triplet states have the same energy, they are *degenerate*. The *multiplicity* of a state can generally be described by $M = 2S + 1$, where singlet states have $M = 1$ and triplet states $M = 3$.

The two-electron system is an important example since the photophysical properties of molecules mainly are characterized by the valence electrons in the highest occupied molecular orbital (HOMO) and the lowest unoccupied molecular orbital (LUMO). Figure 2.1 shows a schematic illustration of a two-electron system in three different states, a singlet ground state, and the two different excited states. It is most common that molecules have a ground state where all orbitals up to, and including, the HOMO level are filled with two electrons of opposite spin. Subsequently, most molecules have singlet ground states. However, there are exceptions, for example molecular oxygen which has a triplet ground state. The HOMO for oxygen is degenerate, and according to *Hund's rule*, these molecular orbitals are each occupied singly with *unpaired* electrons before any orbital is filled with two electrons. Hence, for ground state oxygen, two electrons with the same spin occupy one HOMO each.

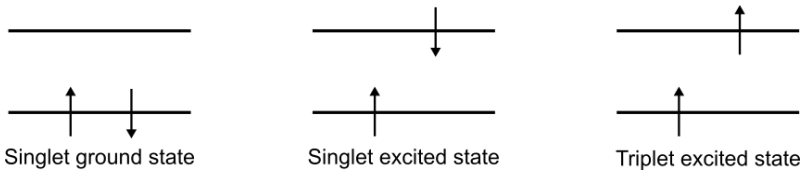



**Figure 2.1:** Schematics of electron spin in a two-electron system.

### 2.1.2 Decay processes

When a molecule has been excited through the absorption of a photon, there are several different ways for it to decay back to its ground state. If the decay involves the emission of a photon, it could be either *fluorescence* or *phosphorescence*, depending on the nature of the excited state that the radiative emission originates from. Fluorescence is radiative emission of photons from singlet states, while phosphorescence is radiative decay from triplet states.

In addition to the two different types of emission, the decay of an excited state could be non-radiative. A common way to show the different decay possibilities is by a *Jablonski diagram* (Figure 2.2), which illustrates a molecule's states and the transitions between them. The singlet ground state is denoted $S_0$, and the singlet excited states $S_1$, $S_2$, etc. Similarly, the excited triplet states are denoted $T_1$, $T_2$, etc. At each of these electronic states, the molecule can be in several vibrational energy levels, illustrated with the thin horizontal lines. When a molecule is relaxed to a vibrational level of lower energy it is called vibrational relaxation (VR). Together with internal conversion (IC), VR form a pathway for non-radiative decay between singlet states.

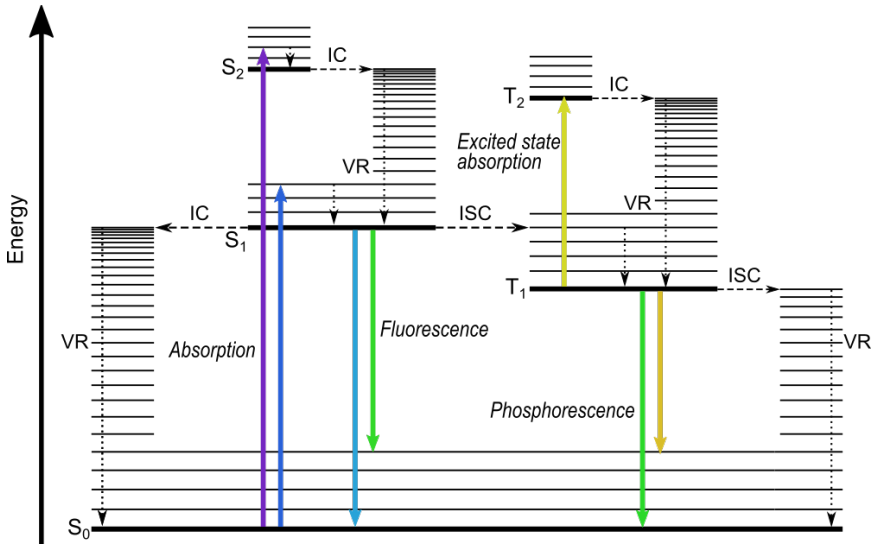



**Figure 2.2:** Jablonski diagram. Thick horizontal lines represent electronic energy levels, $S_i$ and $T_i$ denotes singlet and triplet energy levels. Thin horizontal lines correspond to vibrational levels. Vibrational relaxation (VR) is depicted by vertical, dotted arrows, internal conversion (IC) and intersystem crossing (ISC) by dashed, horizontal arrows. Colored, vertical arrows represent events involving the absorption or emission of a photon.

Vibrational relaxation is very rapid. Therefore, fluorescence mostly occurs from the lowest vibrational level of $S_1$. The same applies for intersystem crossing (ISC), which is the transition from a singlet to a triplet state, or the opposite. Intersystem crossing is a spin forbidden transition, as it includes a change in electron spin for the excited electron. Thus, the formation of triplet excited states is less probable than formation of singlet excited states. However, in some molecules containing heavy atoms, as for instance bromine or iodine, ISC is favored and therefore, the formation of triplet excited states more likely.[14]

Triplet excited states rapidly relax to the lowest vibrational level of the triplet, from which phosphorescence could occur. Like ISC, phosphorescence is a spin forbidden transition. As a result, the rate constants for phosphorescence are in general several magnitudes smaller compared to those of fluorescence. Consequently, the phosphorescence is generally slower and its intensity lower. Triplet excited states can also decay non-radiative through ISC and VR.

### 2.1.3 Some useful concepts

The relative rate of a specific process can be expressed by its *quantum yield* (QY). One of the more common is the fluorescence quantum yield, $\Phi_f$, defined as the ratio of the number of photons emitted to the number of photons absorbed. The QY of fluorescence can also be described as

$$\Phi_F = \frac{k_F}{\sum k} \tag{2.5}$$

where $k_F$ is the rate of fluorescence and $\sum k$ the sum of the rates of all decay processes proceeding from the singlet excited stated $S_1$. Similarly, the quantum yield can be expressed for other processes as well, for example $\Phi_{ph}$, the QY of phosphorescence. It is also possible to describe the decay processes using lifetimes instead of rate constants. The lifetime ($\tau$) is defined as the average time spent in the excited state and takes the inverse value of the sum of the rates of all decay processes proceeding from the excited state,

$$\tau = \frac{1}{\sum k} \tag{2.6}$$

By examining the Jablonski diagram in Figure 2.2 it can be noticed that the energies of the absorption and the fluorescence are not the same. One reason for this is the previously mentioned very quick VR which results in most fluorescence occurring from the lowest vibrational level of $S_1$. Another is that it is common for fluorescence to decay to higher vibrational levels of $S_0$ (e.g. as the green fluorescence arrow in Figure 2.2). The *Stokes shift* is defined as the position difference of band maxima between the absorption and emission spectra, and can therefore be used as a descriptor of the energy loss between absorption and emission. In the case of photon upconversion (UC), where the emission is of higher energy than the absorption, the apparent *anti*-Stokes shift can instead describe the general energy gain of the process.

Another important concept when discussing fluorescence and phosphorescence is *quenching*. Quenching is a process resulting in reduced emission intensity and de-

creased decay lifetime, and there are several different things that may cause quenching. One example is ISC, as it gives a non-radiative pathway to the ground state. Quenching can also follow by the contact of some atoms or molecules, which are then called quenchers. Two common examples are iodine ions and oxygen.[14] Molecular oxygen easily quenches triplet excited states in surrounding compounds, as it itself has a triplet ground state. Therefore, an oxygen free atmosphere is typically necessary to see and measure phosphorescence, or when triplet states are part of the desired photophysical process.

## 2.2 Photon upconversion

The concept of photon UC was briefly described in the introduction but shall here be explained more thoroughly. The process used in this study utilizes the interaction of two types of molecules to combine the energy from two incoming photons into one emitted UC photon. The two types of compounds are donor molecules called sensitizers, and acceptor molecules called annihilators. The process, called *sensitized triplet-triplet annihilation photon upconversion* (sTTA-UC), consists of two events where energy is transferred between molecules. The first, called *triplet energy transfer* (TET), transfers energy from sensitizer to annihilator. The second mechanism occurs between two annihilators and is called *triplet-triplet annihilation* (TTA).

### 2.2.1 Dexter energy transfer

The transfer of energy between sensitizer and annihilator occurs as the excitation moves from one triplet state to another, thus called TET. This energy transfer is of a type named *Dexter energy transfer* (DET), a mechanism available also for singlet energy transfer. During the DET event, there is a virtual electron exchange between the interacting molecules. The donor molecule, $D$, transfers an electron in an excited state, while the acceptor molecule, $A$, transfers a ground state electron. In this way, energy has been transported from the donor to the acceptor as the transfer of the excitation. The TET can also be expressed as

$$^3D^* + {}^1A \rightarrow {}^1D + {}^3A^* \tag{2.7}$$

where the asterisk denotes an excited state, and the superscript numbers denote the spin multiplicity.

The interacting molecules must be in very close proximity to each other, as an orbital overlap is necessary for the DET to take place. In fluid solution, the energy transfer occurs through collisions between the species, as a result of diffusion in the liquid. It is therefore promoted by high concentrations. The TET process can also be described as a type of quenching since the energy transfer from sensitizer to annihilator deexcites the sensitizer without the direct emission of a photon. The efficiency of a diffusion controlled quenching process is described by Equation 2.8, the well-known Stern-Volmer equation.[14]

$$\frac{F_D}{F_{DA}} = \frac{\tau_D}{\tau_{DA}} = 1 + k_q \tau_D [Q] \tag{2.8}$$

Here, $F_i$ are emission intensities, $\tau_i$ excited state lifetimes, $k_q$ is the bimolecular quenching constant and $[Q]$ the quencher concentration. The subscripts $D$ and $DA$ correspond to solution with only donor and solution with both donor and acceptor, respectively. As mentioned above, the TET event is a type of quenching and Equation 2.8 can therefore be used in the analysis of the TET rate and efficiency. Then $k_q$ is the rate of energy transfer, $k_{TET}$, and $[Q]$ is the concentration of annihilator, $[A]$. Thus, an estimation of $k_{TET}$ may be done by measuring the quenching of donor emission or difference in excited state lifetime with respect to $[A]$. Subsequently, the efficiency of the triplet energy transfer, $\Phi_{TET}$, can be expressed as

$$\Phi_{TET} = 1 - \frac{F_{DA}}{F_D} = 1 - \frac{\tau_{DA}}{\tau_D} = 1 - \frac{1}{1 + k_{TET}\tau_D[A]} \tag{2.9}$$

### 2.2.2 Triplet-triplet annihilation

The TTA mechanism could possibly be called the heart of the UC process, as perhaps implied by the name sTTA-UC. The process is illustrated in Figure 2.3. It starts with two sensitizers that absorbs one photon each, promoting the sensitizers to their first excited singlet state, denoted $S_1$. Through ISC the excitations are transferred to the triplet excited states, $T_1$. Then, the sensitizers interact with the annihilators via TET. The sensitizers, which are in their triplet excited state, acts as donors and the ground state annihilators as acceptors. Subsequently, two triplet excited annihilators are created. These then interact with each other via TTA, promoting one annihilator to the singlet excited state while the other annihilator will return to the singlet ground state. At last the sTTA-UC process is completed when the singlet excited annihilator relaxes back to the ground state by the emission of a photon.

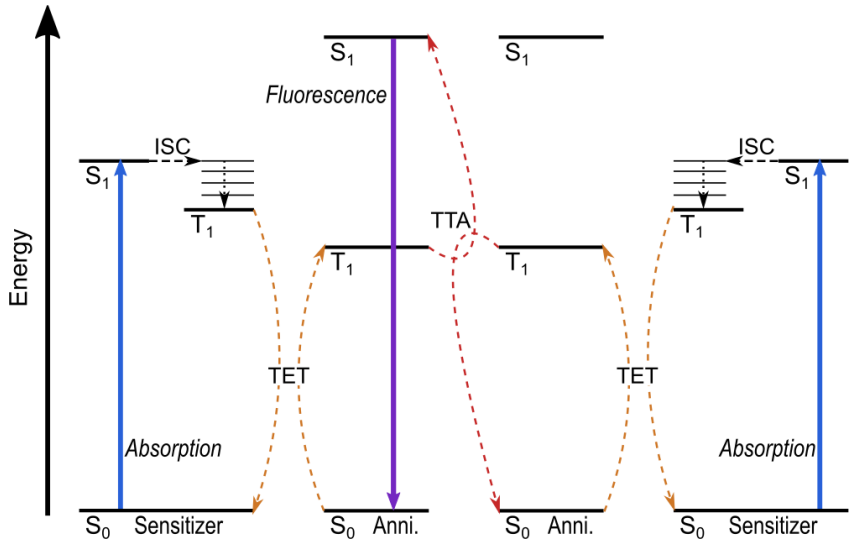



**Figure 2.3:** The process of sTTA-UC. Firstly, the sensitizers are excited by the absorption of a photon. They then experience ISC creating triplet excited sensitizers. The excitations are transferred to the annihilators by TET. Two annihilators interact through TTA, creating a singlet excited annihilator. At last, the annihilator emits a photon with higher energy then the photons originally absorbed by the sensitizers.

### 2.2.3 Upconversion efficiency

Of great interest for this project is the efficiency of the upconversion process. However, in literature, there is some variety in the terminology for TTA-UC, particularly regarding the upconversion quantum yield, $\Phi_{UC}$. It is most common that $\Phi_{UC}$ describes the emission QY, defined as the ratio between emitted UC photons and photons absorbed by the sensitizer. Though sometimes, $\Phi_{UC}$ have been used to describe the normalized yield, which is used to scale the theoretical efficiency from 50 to 100 %. Attempts to sort out the confusion have been made, in particular by Zhou et al.[15] who suggest that if normalization is used, the result should be labeled as $\eta_{UC}$, the normalized upconversion emission efficiency, where $\eta_{UC} = 2 \times \Phi_{UC}$.

Furthermore, Zhou et al. suggest a different definition for $\Phi_{UC}$: the ratio between UC photons *observed* and sensitizers in the singlet excited state (the latter is assumed to equal the earlier description: photons absorbed by the sensitizers). It is this definition of the observed, or external, quantum yield that will be used in this thesis. However, there is another parameter described by Zhou et al. which will be of greater interest for this project as it describes the intrinsic ability for effective UC. The internal quantum yield, or the QY of photons generated, $\Phi_{UC,g}$, is defined as the ratio between UC photons *generated* and sensitizers in the singlet excited state. $\Phi_{UC,g}$ may also be described as

$$\Phi_{UC,g} = f \times \Phi_{ISC} \times \Phi_{TET} \times \Phi_{TTA} \times \Phi_F \tag{2.10}$$

where $\Phi_i$ is the efficiency of the different steps of the TTA-UC process and $f$ is a probability factor related to spin statistics. $\Phi_{ISC}$, $\Phi_{TET}$ and $\Phi_F$ may all approach unity, but since the TTA process requires two low-energy photons to afford one high-energy photon, $\Phi_{TTA}$ (and subsequently also $\Phi_{UC,g}$) has a theoretical maximum of 50 %.

#### 2.2.3.1 Spin statistical factor

The spin-statistical factor $f$ gives the probability that a singlet excited state is created through TTA. During the TTA event, two triplet excited annihilators first form an encounter complex, which can be either of singlet, triplet, or quintet multiplicity. Equation 2.11 show the pathway and possible products of these encounter complexes, where one and two asterisks denote first and higher excited states, respectively, and the superscript numbers denote spin multiplicity.

$$^3A^* + {}^3A^* \rightleftharpoons \begin{cases} {}^1|A\cdots A|^* \rightarrow {}^1A + {}^1A^* \\ {}^3|A\cdots A|^* \rightarrow {}^1A + {}^3A^{**} \\ {}^5|A\cdots A|^* \end{cases} \tag{2.11}$$

The probabilities of the formation of the three different states are related to their respective spin multiplicity, and thus, the outcome of interacting triplet pairs is singlet, triplet or quintet states with 1:3:5 relative ratio. It is only the emissive singlet state that is the desired product for TTA-UC, and the other states can

therefore be viewed as by-products. Hence, the theoretical maximum for $\Phi_{UC}$ would be $0.5 \times 1/9 = 5.6$ %. However, as mentioned in the introduction, upconversion efficiencies far beyond this have been reported.[13]

There are several reasons to why the spin statistical limit can be broken. Firstly, quintet states commonly have very high energies and thus are typically inaccessible. The quintet complex therefore dissociates back to the two initial triplet molecules.[16] Secondly, the products following the triplet encounter complex can partly be reused. The triplet product $^3A^{**}$ is in its second excited triplet state, previously denoted $T_2$. The high energy triplet usually quickly decays back to the first excited triplet state, hence one of the two original $^3A^*$ has been recycled.[16] Subsequently, if four triplet pairs undergo TTA, five triplet states in total will be destroyed; two when one pair forms a singlet, and one each for the three pairs resulting in a triplet. Since two of these five triplets contribute to the desired formation of a singlet excited state, it leads to a $f$ value of 2/5, and 20 % as a new spin statistical limit for $\Phi_{UC}$.

Even higher values of the spin statistical factor are possible. If the $T_2$ state have a significantly higher energy than the $S_1$ state, the distribution of produced singlets and triplets may not be purely statistical.[17] This is especially the case when the energy of the $T_2$ state exceeds the double of the energy of the $T_1$ state, where the values for $f$ may even approach unity.[16]

In a recent study by Bossanyi et al.[18], it is shown that the production ratio for singlet, triplet and quintet encounter complexes is not as simple as the common 1:3:5. This ratio assumes that the annihilating triplets form triplet-pair states with a strong electronic coupling, but Bossanyi et al. show that the triplet-pair states are weakly exchange-coupled. They also showed that the relative orientation of the two annihilating molecules affects $f$, going from 2/5 for perpendicular molecules to 2/3 for parallel molecules. It is also suggested that $f$ may approach unity even if $[2 \times E(T_1) - E(T_2)]$ is close to zero, due to a process called high-level reversed intersystem crossing (HL-rISC), which is a transition from $T_2$ to $S_1$.

#### 2.2.3.2 Excitation intensity

Another parameter that affects the efficiency of the UC process is the intensity of the excitation light, $I_{EX}$. Higher light intensity will support the creation of more excited states, firstly singlet excited sensitizers, and subsequently triplet excited sensitizers and annihilators. Quite intuitively, more excitations lead to more UC emission, but there is a certain value of importance called the *intensity threshold*.

As mentioned before, TET is a diffusion-controlled process and is therefore promoted by high concentrations. This is also the case for TTA, for which to occur, two triplet excited state annihilators must collide. A high annihilator concentration, $[A]$, is therefore a prerequisite for effective UC. The light intensity controls the production, and thereby also the concentration of *triplet excited* annihilators, $[^3A^*]$. At low $I_{EX}$, $[^3A^*]$ is relatively low and TTA will compete with other decay processes. As a result, the UC emission will have a quadratic dependence on $I_{EX}$, and $\Phi_{UC}$ will have a linear dependence on $I_{EX}$. At high excitation intensities, TTA dominates, and the UC emission linearly depend on $I_{EX}$, while $\Phi_{UC}$ is independent

of light intensity. The intensity threshold ($I_{th}$) is the value at which the transition from quadratic to linear dependence occur,[19] and can be described by

$$I_{th} = \frac{k_T^2}{2k_{TTA}\alpha[^1S]} \tag{2.12}$$

where $k_T$ and $k_{TTA}$ are the rates of annihilator triplet decay and TTA, respectively, $\alpha$ is the absorption cross-section of the sensitizer and $[^1S]$ is the concentration of ground-state sensitizer.

The solar flux at the Earth's surface is only a few mW/cm$^2$ for a small wavelength range in the region of interest for vis-to-UV UC. If the ambition is to utilize sunlight as the energy source for the TTA-UC process, it is therefore beneficial for the system to have as low as possible $I_{th}$.

## 2.3 TADF sensitizer

The sensitizer selected for this project is a molecule which exhibit *thermally activated delayed fluorescence* (TADF). Employed as TTA-UC sensitizers, TADF compounds are a relatively new group of molecules, first reported in 2015.[20] Since then several systems have been developed, upconverting light from different parts of the light spectrum.[21, 22, 23, 24] TADF compounds have very small energy gaps between their excited singlet and triplet states, $\Delta E_{S-T}$, enabling *reversed intersystem crossing* (rISC), the transition from the triplet excited state to the singlet excited state. When fluorescence follows ISC and rISC it is delayed since the lifetime of the triplet state is typically several magnitudes longer than the lifetime of the singlet excited state. Fluorescence can also occur directly after the excitation, then called prompt fluorescence (PF), as opposed to the delayed fluorescence (DF).

The different decay processes for a TADF molecule along with the process of sTTA-UC are illustrated by a Jablonski diagram in Figure 2.4. The main differences from the sTTA-UC process with a classical sensitizer (Figure 2.3) are the small energy gap between $S_1$ and $T_1$, and subsequently, the additional accessible rISC. The endothermic transition is enabled through absorption of thermal energy from the surroundings, thus called thermally activated. The last significant difference for the TADF sensitizer is that it has two types of emissive decay from $S_1$. Since originating from the same electronic state, PF and DF have the same energies and wavelengths. The only difference is the time between the excitation and the emission, expressed as the lifetimes $\tau_{PF}$ and $\tau_{DF}$. The PF lifetime is governed by the lifetime of the singlet excited state, in other words, $\tau_{PF} = \tau_S$. Similarly, the lifetime of the triplet excited state determines $\tau_{DF}$. The efficiency of the prompt and delayed fluorescence is denoted as $\Phi_{PF}$ and $\Phi_{DF}$, respectively. Like all quantum yields, $\Phi_i$ is the fraction of the excited molecules taking pathway $i$.

Apart from being one of the main characteristics of TADF compounds, the small $\Delta E_{S-T}$ is advantageous as it leads to smaller amounts of energy lost during the ISC event, and thus might contribute to a larger anti-Stokes shift for the sTTA-UC system. However, to be an efficient sensitizer, it is required that the TADF compound has a large ISC efficiency, $\Phi_{ISC}$, to promote the production of as many

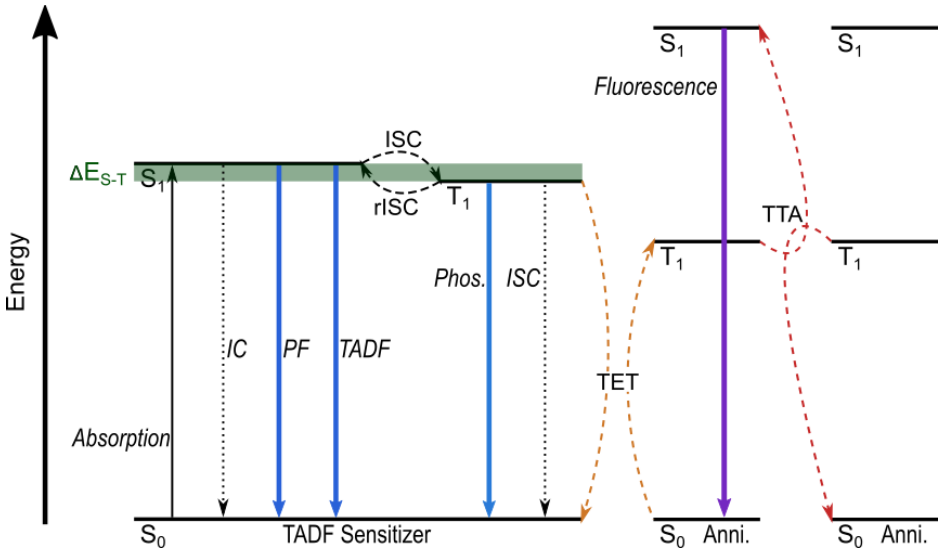



**Figure 2.4:** Jablonski diagram depicting the different decay processes for a TADF compound alongside the process of sTTA-UC using a TADF compound as sensitizer.

triplets as possible. Likewise, it is preferable that $\Phi_{rISC}$ is small. When non-radiative decay from $S_1$ is neglected, $\Phi_{ISC}$ can be estimated according to Equation 2.13.[25] Consequently, a low $\Phi_{PF}$ and a high $\Phi_{DF}$ is desired.

$$\Phi_{ISC} = 1 - \Phi_{PF} \tag{2.13}$$

The sensitizer used in this project is 2,3,5,6-tetra(9H-carbazol-9-yl)benzonitrile (4CzBN), its molecular structure is shown in Figure 2.5. 4CzBN is a blue emitting, purely organic molecule developed by Zhang et al.[26] TADF materials contain electron donating and electron accepting groups, and the small $\Delta E_{S-T}$ results from a high level of intramolecular charge transfer, a characteristic of TADF compounds. In 4CzBN the four carbazolyl groups act as electron donors, while the central benzonitrile group acts as electron acceptor. Zhang et al. reported a measured $\Delta E_{S-T}$ of 0.30 eV, as well as photoluminescence efficiencies of 0.10 and 0.39 for prompt and delayed fluorescence, respectively. A calculated triplet state energy of 2.70 eV was also reported.

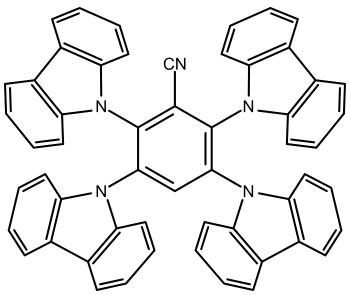



**Figure 2.5:** The molecular structure of the sensitizer 4CzBN.

### 2.3.1 TET rate and efficiency for TADF sensitizers

In the case of a TADF sensitizer, the calculation of the TET rate and efficiency is not as straight forward as for more traditional sensitizers with larger $\Delta E_{S-T}$. To achieve an efficient sTTA-UC process it is favorable if the TET outcompetes the other decay processes available for triplet excited sensitizers. When the sensitizer is a TADF compound, there is one additional competing transition proceeding from the $T_1$ state, the rISC. Furthermore, the ISC and rISC creates an equilibrium between the singlet and triplet excited states, which is perturbed when the TADF compound is part of a TTA-UC system due to the presence of the annihilators and consequent TET.

In previous studies, two different approaches have occurred for the determination of the TET efficiency. The first is to measure the quenching of donor emission,[21] and the second method is to measure the change of $\tau_{DF}$ upon addition of annihilator.[23] Both methods originates from the Stern Volmer equation (Equation 2.8) and are described in Section 2.2.1 above. However, due to the perturbed ISC/rISC equilibrium, the expression for $\Phi_{TET}$ presented in Equation 2.9 is not correct. To make an accurate expression, Olesund et al.[27] define the TET efficiency so that it includes the ISC event. For TADF sensitizers, the $\Phi_{TET}$ can be expressed as

$$\Phi_{TET} = \frac{k_{ISC}\, k_{TET}\, [Q]}{(k_{rISC} + k_T)(k_F + k_{nr,S} + k_{ISC}) - k_{ISC}\, k_{rISC}} \tag{2.14}$$

where $k_i$ is the rate constant for event $i$, except $k_T = k_{ph} + k_{nr,T} + k_{TET}[Q]$ which is the sum of the rates of all decay processes proceeding from the first triplet excited state. The subscripts $ph/nr, T$ and $F/nr, S$ denote radiative/non-radiative decay from the first triplet excited state and the first singlet excited state, respectively.

Although possible, it requires a lot of work to evaluate the expression in Equation 2.14 as all the rate constants then would need to be determined. An approximate method is therefore desired, and Olesund et al. performed simulations to investigate the validity of the two previously used methods described above. The results showed that it is a good approximation to use the quenching of steady-state emission for TADF sensitizers with small $\Delta E_{S-T}$ (<0.1 eV), while for compounds with larger $\Delta E_{S-T}$ (>0.1 eV) it is more accurate to use the lifetime of the delayed component. As $\Delta E_{S-T}$ is 0.3 eV for 4CzBN, it is assumed that only evaluating the change of $\tau_{DF}$ as an approximate method will give a sufficiently good estimate of $\Phi_{TET}$. Hence, the TET rate may be estimated by probing the change in DF lifetime with respect to annihilator concentration according to

$$\frac{\tau_{DF,0}}{\tau_{DF}} - 1 = k_{TET}\, \tau_{DF,0}\, [A] \tag{2.15}$$

Subsequently, the TET efficiency can be calculated according to Equation 2.16, where $k_T = k_{ph} + k_{nr,T} = 1/\tau_{DF,0}$. For further explanations and derivation details see Appendix A.

$$\Phi_{TET} = \Phi_{ISC} \frac{k_{TET}[A]}{k_T + k_{TET}[A]} \tag{2.16}$$

## 2.4 Annihilators

If a compound is to be appropriate as annihilator in a sTTA-UC system, there are several molecular characteristics required. As the aim of this project is to achieve vis-to-UV UC, the most fundamental is being a UV emitter. To make the TTA event feasible, the energy of the singlet excited state should be less than twice the energy of the triplet excited state, $E(S_1) < 2 \times E(T_1)$. However, to minimize energy losses and promote high anti-Stokes shifts, it is advantageous if the difference is relatively small. For the same reason it is preferable that $E(T_1)$ of the annihilators is just slightly lower than that of the sensitizer, although too small driving forces may affect the efficiency of the system. Another requirement for efficient UC is a high fluorescence QY as this directly affects the efficiency of the total system (see Equation 2.10).

In this project six different annihilators have been used, all presented in Figure 2.6. Possibly the most prominent UV emitting annihilator is 2,5-diphenyloxazole (PPO), which has previously been combined with several different sensitizers.[9, 24, 28, 29] The highest achieved UC quantum yield so far is 10.4 % which was accomplished by coupling PPO with a cadmium sulfide nanocrystal sensitizer.[11] Another annihilator which has succeeded to surpass 10 % UC efficiency is 1,4-bis((2,5triisopropyl-silyl)ethynyl)naphthalene (TIPS-naph). First synthesized by Harada et al.[10] in 2020 it was combined with an iridium sensitizer, and it has later shown a similar efficiency coupled with a sensitizer free from heavy metals.[12]

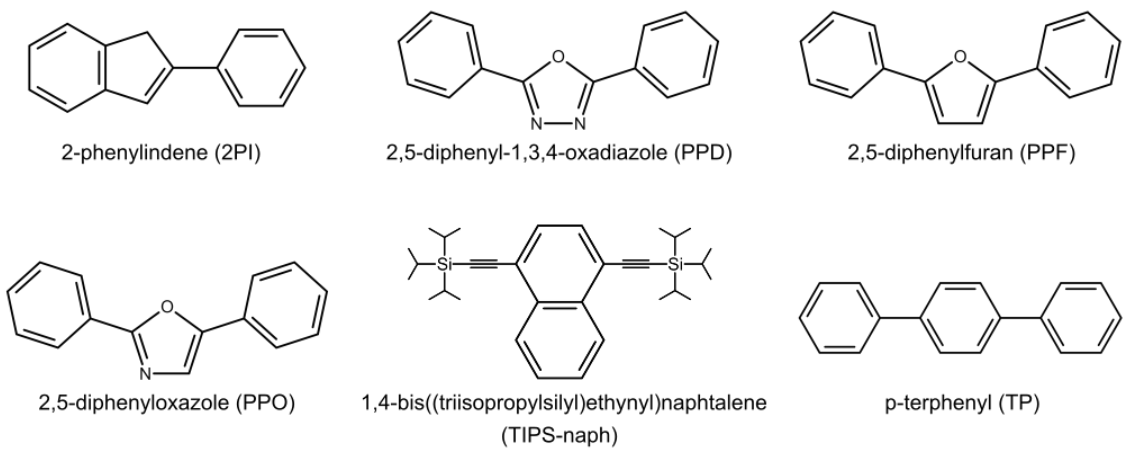



**Figure 2.6:** The molecular structures, full names and acronyms of the annihilators.

Although quite commonly applied as an annihilator for sTTA-UC, the UC quantum yield of p-terphenyl (TP) have yet been low.[11, 21, 24] A maximal 3.8 % UC quantum yield was obtained in a system with a TADF sensitizer.[30] An even lower efficiency, only 0.2 %, have been reported for 2,5-diphenyl-1,3,4-oxadiazole (PPD).[11] The last two annihilators, 2,5-diphenylfuran (PPF) and 2-phenylindene (2PI), have as far as I know not been used in a sTTA-UC system before.

As mentioned above, the annihilator triplet state energy is a key factor for the viability and efficiency of the sTTA-UC system. Literature values of the triplet state

energies are shown in Table 2.1. Apart from showing a range in upconversion QY, the six annihilators have a broad span of triplet energies with a maximal difference of 0.70 eV.

**Table 2.1:** Triplet excited state energies from literature.

| | PPD | TP | PPO | PPF | 2PI | TIPS-naph |
|---|---|---|---|---|---|---|
| $T_1$ (eV) | 2.82[a] | 2.62[b] | 2.40[b] | 2.28[c] | 2.22[b] | 2.12[d] |

[a]Reference [31]. [b]Reference [32]. [c]Reference [27]. [d]Reference [10].

# 3
# Methods

The aim of this chapter is to describe the experimental techniques and calculations used within this thesis. Many spectroscopic measurements were conducted in order to achieve the aim of the project, increased knowledge of the annihilator's characteristics impact on the UC efficiency. Subsequently, the results of the measurements were used to calculate different parameters that are known to affect the UC process.

## 3.1 Steady-state absorption spectroscopy

Mostly applied in the UV-visible region, steady-state absorption spectroscopy is a technique used to acquire information about how a compound responds to different wavelengths of light. It may also be used to identify the molecules in a sample and their concentrations. A schematic illustration of the setup for absorption measurements is shown in Figure 3.1. The main components of the spectrometer are light source, monochromator and detector. The monochromator contains a dispersion device, for example a diffraction grating, which splits the incoming light into different angles depending on wavelength. The exit slit is used to select a narrow range of light allowed out from the monochromator. A beam splitter divides the light into two beams, one of which is reflected to a reference detector. The other beam passes through the sample before reaching the detector. The reference detector measures the incident light intensity, $I_0$, while the sample detector measures the intensity of the transmitted light, $I$.

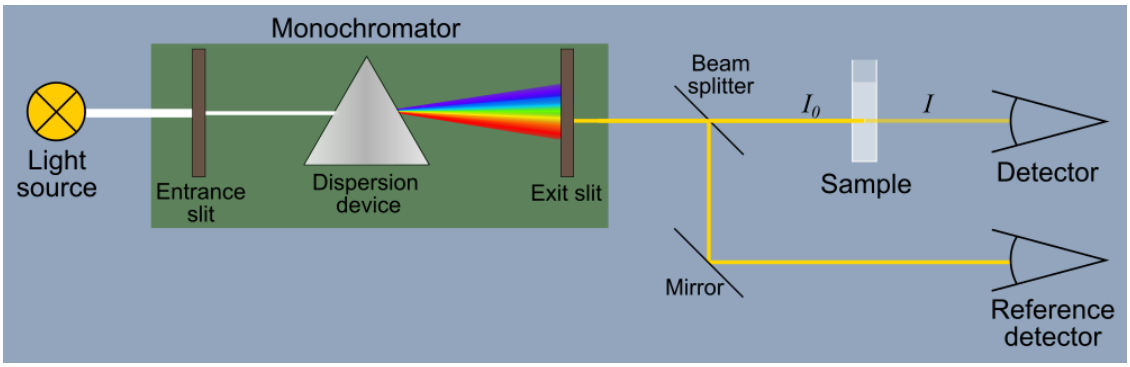



**Figure 3.1:** Schematic illustration of the experimental setup for absorption measurements.

If the sample absorbs light of the wavelength selected by the monochromator, the light intensity will be lower after it has passed through the sample. The ratio of

the light intensities can be used to calculate the absorbance, $A$, according to

$$A = -\log_{10} \frac{I}{I_0} \tag{3.1}$$

By adjusting the monochromator, the absorbance can be measured over a range of wavelengths and an absorption spectrum can be created. At a certain wavelength, the absorbance is proportional to the concentration of the absorbing compound according to *Lambert-Beer's law*,

$$A(\lambda) = \epsilon(\lambda)cl \tag{3.2}$$

where $\epsilon$ is the molar absorptivity, also called the extinction coefficient, $c$ the concentration and $l$ the length of the path the light travels through the sample. If the sample contains several species, as is the case for the UC samples, both compounds may absorb light at the same wavelength. Then, the measured absorbance reflects the total fraction of photons absorbed by the sample at that wavelength, dictated by the present species and their respective molar absorptivity and concentration.

## 3.2 Steady-state emission spectroscopy

Molecules that absorb light gain excess energy that may be released as emission as the molecules decay back to their ground state. A schematic illustration of an emission spectrometer is presented in Figure 3.2. The technique used to measure emission has several similarities with absorbance measurements, starting with a light source. Following is a monochromator used to choose the excitation wavelength of the light illuminating the sample. The selected wavelength should be one at which the sample absorbs, chosen by examining the absorption spectrum.

The luminescent sample emits light in all directions, some of it passing into another monochromator. The exit slit of the emission monochromator lets out a narrow wavelength range of light directed towards the detector. The sample detector is typically oriented in a right angle compared to the incident light, to avoid detecting any excitation light and only detect the emission. A reference detector is used to identify and correct for small fluctuations in excitation light intensity.

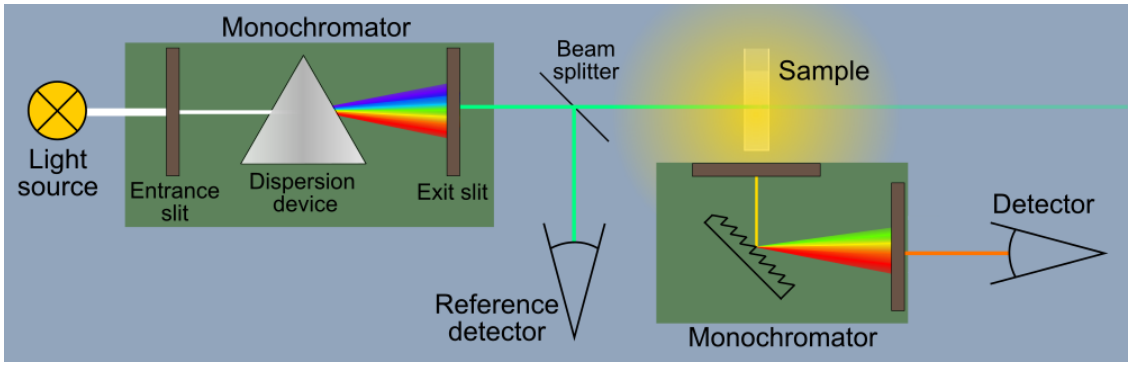



**Figure 3.2:** Schematic illustration of the experimental setup for emission measurements.

An emission spectrum can be produced by letting the second monochromator sweep over a range of wavelengths. By instead selecting a fixed emission wavelength and measure over a range of excitation wavelengths, an excitation spectrum can be constructed. Excitation spectra typically resembles the absorption spectra of the sample, as it shows which wavelengths that lead to emission.

### 3.2.1 Upconversion measurements

The experimental setup used for upconversion emission measurements do not differ much from that used for ordinary steady-state emission. Instead of a non-coherent light source and an excitation monochromator, a laser is often used as excitation source. In this project, a custom-made system with a continuous-wave 405 nm laser was utilized for the UC measurements. The laser beam had a diameter of 0.8 mm, and a maximal power output of 87.3 mW. A notch filter was placed in front of the detector to remove any excitation light scattered in its direction. The excitation light intensity could be somewhat varied using the software belonging to the laser, and further adjusted using a linear variable neutral density (ND) filter. For all measurements conducted to calculate the upconversion quantum yield, the maximal excitation intensity was used. To minimize reabsorption, 2 mm cuvettes were used for all UC measurements, with the shorter path length directed towards the detector.

## 3.3 Time-resolved emission spectroscopy

Time-resolved emission spectroscopy can be used to measure the emissive decay in the time-domain and determine the emission lifetime, $\tau$. The setup for time-resolved measurements is very similar to the one of steady-state measurements, where the main difference is another type of light source and in what manner the emission is detected. For time-resolved spectroscopy, a pulsed excitation light source, usually a laser, is used instead of continuous wave light. Each excitation pulse should be shorter than the time scale of the emission lifetime of interest. In this project, using nanosecond laser excitation, the laser had a pulse frequency of 10 Hz, and a pulse length of approximately 10 ns. The emission is detected during a determined time length following each laser pulse, and the acquired data are compiled into a graph showing the decay of the excited state population.

## 3.4 Calculations and fitting procedures

### 3.4.1 Quantum yields

By utilizing the results from both steady-state absorption and steady-state emission measurements, the emission quantum yield, $\Phi$, can be calculated. A common method to determine $\Phi$ is to compare the sample to a standard with known quantum yield, according to Equation 3.3.[14]

$$\Phi = \Phi_{ref} \frac{F\ A_{ref}\ n^2}{F_{ref}\ A\ n_{ref}^2} \tag{3.3}$$

Here, $F$ is the integrated emission intensity, $A$ the absorbance at the excitation wavelength and $n$ the refractive index of the solvent. The subscript $ref$ refers to the standard sample containing the reference compound.

For the determination of the quantum yield according to Equation 3.3, the sample and the standard should be excited at the same wavelength and the same excitation intensity. The sensitizer and the annihilators absorb light from different wavelengths, and thus, they require different standards to match their respective absorption regions. For the determination of fluorescence quantum yields of the annihilators, p-terphenyl (TP) in cyclohexane was utilized as reference, which absorbs at 225 – 325 nm and has a quantum yield of 0.93.[33] The second standard used in this project was coumarin 153 (C153) in ethanol, which absorbs at 350 – 500 nm and has $\Phi = 0.53$.[34] C153 was used as reference for the determination of the emission quantum yields of the sensitizer and of the UC quantum yields, since 4CzBN was the excited compound in both cases.

When determining the quantum yield, the absorbance should be kept below 0.05 to avoid so called *inner filter effects*.[14] If the absorbance is too high, the intensity of the excitation light may substantially decrease during the pathlength of the sample. A decreasing excitation light intensity throughout the sample means that only a part of the excitation light will reach the point of the sample from which the emission is observed. Thus, when the absorbance exceeds 0.05, the measured emission intensity is no longer proportional to the measured absorbance. Another inner filter effect is re-absorption of emitted photons, which may happen when there is a spectral overlap between the absorption and emission of the sample.

### 3.4.2 Upconversion quantum yields

Two different upconversion quantum yields, defined in Section 2.2.3, are used in this thesis to describe the UC efficiency. The difference between the observed ($\Phi_{UC}$) and generated ($\Phi_{UC,g}$) quantum yield is that the former is dependent on sample properties, like path length and sample holder, and thus describes the number of photons actually reaching the detector. In contrast, $\Phi_{UC,g}$ accounts for optical output losses, such as inner filter effects and scattering, and is a measure of the number of UC photons produced.

Like for the determination of ordinary emission quantum yields, the UC quantum yields were determined by comparing the samples to a reference compound.

However, a slightly different equation was used to calculate the UC quantum yield (Equation 3.4), as Equation 3.3 is only correct if the two absorbances is approximately the same, which was not the case for the UC samples.

$$\Phi_{UC} = \Phi_{ref} \frac{F_{UC}\,(1 - 10^{-A_{ref}})\,n_{UC}^2}{F_{ref}\,(1 - 10^{-A_{UC}})\,n_{ref}^2} \tag{3.4}$$

Both $\Phi_{UC,g}$ and $\Phi_{UC}$ were calculated according to Equation 3.4, where their difference originates from the fitting procedure of the UC emission spectra, and thus, the values of the integrated emission $F_{UC}$. The measured UC spectrum (Figure 3.3, black spectrum) consists of two main parts, the UC emission on the high-energy, left hand side of the spectrum and the prompt fluorescence from 4CzBN on the low-energy, right hand side of the spectrum. An emission spectrum from an optically dilute annihilator sample (a sample of only annihilator) was fitted to match the measured UC spectrum (Figure 3.3, blue spectrum). Thus, the fitted spectrum includes the high-energy end of the spectrum that was not detected at the measurement. As this fitted spectrum relates to the number of UC photons produced, its integrated emission was used to evaluate $\Phi_{UC,g}$. Another fitting was made to evaluate $\Phi_{UC}$, since this time only the observed UC emission should be accounted for (Figure 3.3, red spectrum).

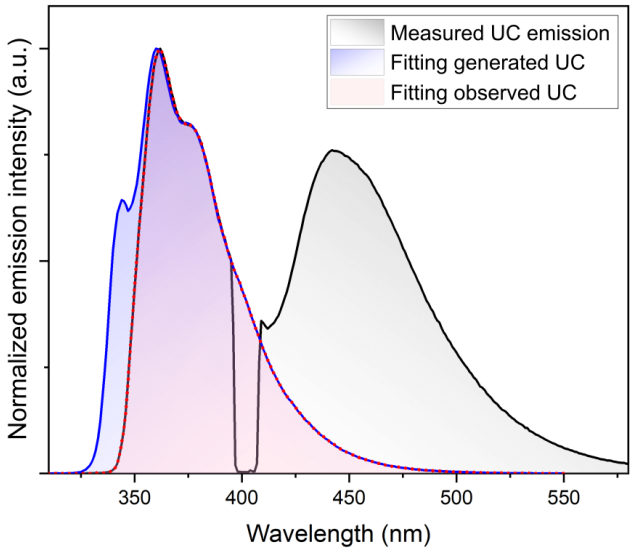



**Figure 3.3:** An example showing the fittings of the UC emission spectra used to calculate $\Phi_{UC,g}$ and $\Phi_{UC}$.

### 3.4.3 Intensity threshold

For UC samples, the intensity of the excitation light was varied to form data plots of the excitation intensity dependence of the UC emission intensity. The plots were done with double logarithmic scales like the example illustrated in Figure 3.4. The intensity threshold ($I_{th}$) was obtained at the intersection of two lines respectively fitted to the experimental data points in the low and high excitation intensity regimes (in turn corresponding to quadratic and linear excitation intensity dependence).

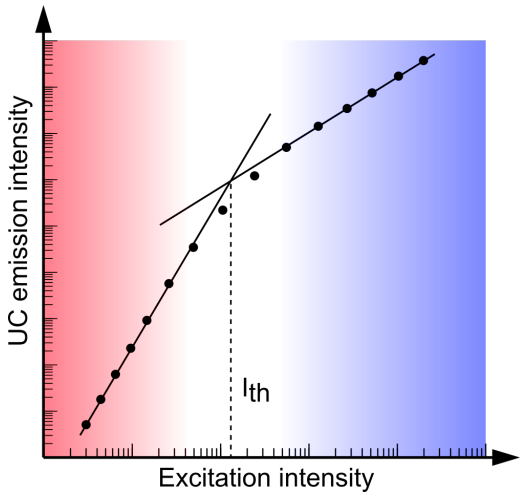



**Figure 3.4:** Illustrative example of excitation intensity dependence of UC emission intensity in a double logarithmic plot and a methodology to obtain the intensity threshold ($I_{th}$). The red and blue shaded areas indicate the regions of quadratic and linear excitation intensity dependence, respectively.

### 3.4.4 Annihilator triplet lifetimes

The triplet lifetime of the annihilator is an important parameter as longer lifetimes promote more efficient annihilation. The annihilator triplet state may decay through phosphorescence or non-radiative (ISC and VR), both processes obeying first-order kinetics. It may also decay through TTA, which is a second-order process since two molecules participate in the TTA event.

The lifetimes were determined using time-resolved measurements, and to regard both first-order and second-order decay, a fitting procedure based on Equation 3.5 was used.[35, 36]

$$I(t) \propto [^3A^*]^n = \left( [^3A^*]_0 \frac{1-\beta}{\exp(t/\tau_T) - \beta} \right)^n \tag{3.5}$$

Here, $I(t)$ is the emission intensity, $[^3A^*]$ the concentration of triplet excited annihilators, $\tau_T$ the triplet state lifetime, and $\beta$ and $n$ are dimensionless parameters. If the measured emission is a result of a decay process obeying first-order kinetics, the emission intensity is proportional to the concentration of annihilator triplets, and then, $n = 1$. This is the case for phosphorescence and TADF as both are emission from first-order channels, the first direct emission from the triplet state, and the second emission from the singlet excited state following rISC. If instead, the measured emission obeys second-order kinetics, the emission intensity is proportional to the square of the annihilator triplet concentration and $n = 2$. When the triplet lifetime of the annihilators is to be determined, the UC emission is measured. Since the UC emission is a result of second-order TTA, $n = 2$ during the fittings.

The other dimensionless parameter, $\beta$, describes the fraction of triplets initially decaying by second-order channels, namely TTA. $\beta$ is defined as

$$\beta = \frac{2k_{TTA}[^3A^*]_0}{k_T + 2k_{TTA}[^3A^*]_0}, \; 0 < \beta < 1 \tag{3.6}$$

where $k_{TTA}$ and $k_T$ ($= 1/\tau_T$) are the rate constants for TTA and first order intrinsic triplet decay, respectively, and $[^3A^*]_0$ is the initial concentration of triplet excited annihilators. $\beta = 0$ means that all initial triplet decay proceeds through first-order channels, and $\beta = 1$ that all initial decay is of second-order.

The fraction of triplets initially decaying by second-order channels, $\beta$, depends upon the initial concentration of excited triplets, which in turn depends on the excitation intensity. Therefore, time-resolved measurements were conducted at different excitation intensities, and the results were globally fitted according to Equation 3.5. The fittings were done using a shared triplet lifetime, but individual $\beta$ for each trace.

# 4

# Results & Discussion

The following chapter presents and discusses the main results and findings of this thesis project. Photophysical properties of the investigated molecules, both the sensitizer and the six annihilators, are displayed first. Rates, lifetimes, and other parameters important for TTA-UC are presented before showing the UC quantum yields and discussing possible causes for why some annihilators gave higher efficiencies than others.

## 4.1 Sensitizer photophysical characterisation

Normalized absorption and emission spectra of the sensitizer 4CzBN are presented in Figure 4.1. The fluorescence was measured at room temperature in THF, and the phosphorescence at 78 K in 2-metyl-THF. With an absorption onset at around 430 nm, 4CzBN was expected to easily be excited by a 405 nm commercial diode laser (Coherent OBIS). A strong absorption peak is evident at approximately 330 nm, and the impact this absorption feature will have on the high-energy UC photons will be shown further below.

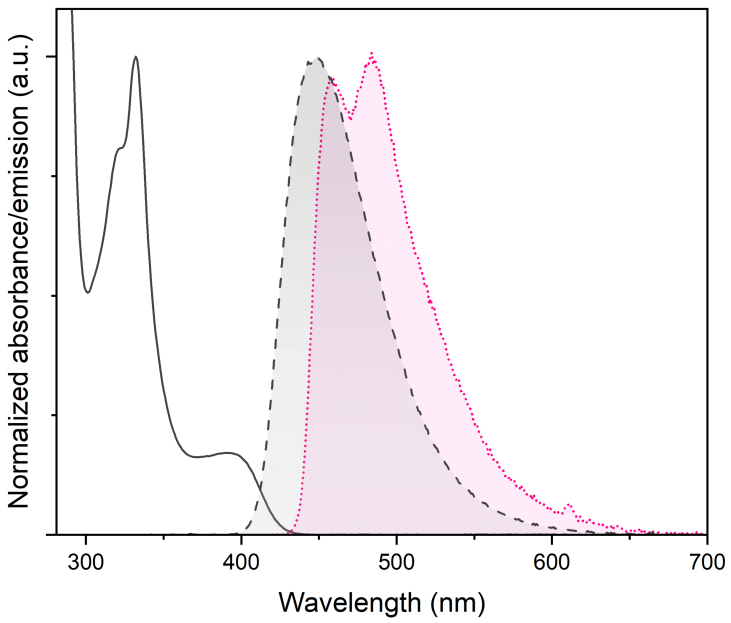



**Figure 4.1:** Normalized absorption (solid), fluorescence (dashed) and phosphorescence (dotted pink) spectra of the sensitizer 4CzBN.

The fluorescence quantum yield of the prompt component ($\Phi_{PF}$) was determined using air-saturated samples, while measurements on oxygen-free samples were conducted to determine the total fluorescence quantum yield ($\Phi_F$). Both quantum yields were determined relative to C153 in air-saturated ethanol. Three samples of each were analyzed and showed only small variations between the samples. However, the presented results are based on the mean values of the measurements, resulting in 0.10 and 0.56 for $\Phi_{PF}$ and $\Phi_F$, respectively. Subsequently, $\Phi_{DF}$ could be determined to 0.46, and the ISC efficiency ($\Phi_{ISC}$) as 0.90 (according to Equation 2.13). The results are in good agreement with previous studies,[26] and are summarized in Table 4.1. The table also displays the lifetime of the delayed component ($\tau_{DF}$) and the energy of the first singlet ($S_1$) and triplet ($T_1$) excited states. The lifetime was calculated from measurements of oxygen-free samples using nanosecond laser excitation. The $S_1$ energy was determined from the intersection of the normalized absorption and fluorescence spectra, and the $T_1$ energy from the position of the highest energy peak in the phosphorescence spectrum.

**Table 4.1:** Photophysical characteristics of the sensitizer 4CzBN.

| | $\Phi_{PF}$ | $\Phi_{DF}$ | $\tau_{DF}$ ($\mu$s) | $\Phi_{ISC}$ | $S_1$ (eV) | $T_1$ (eV) |
|---|---|---|---|---|---|---|
| 4CzBN | 0.10 | 0.46 | 59.3 | 0.90 | 3.01 | 2.71 |

## 4.2 Annihilator photophysical characterization

The characterization of the UV emitters started with measuring absorption and emission spectra for all compounds, which are presented in Figure 4.2. All annihilators emit UV light, but there is quite a difference in how far into the UV-region the emission spectra stretch. This variation can more clearly be described by the difference in energy of the first singlet excited state, which are determined from the intersection of the normalized absorption and fluorescence spectra. The singlet excited state energies are given in Table 4.2, and span from 3.5 to 4.0 eV. As mentioned in Section 2.4, higher singlet excited state energies give larger apparent anti-Stokes shift, but there are other aspects also worth taking into consideration. For easier evaluation, the triplet excited state energies from literature presented previously in

**Table 4.2:** Photophysical characteristics of the annihilators.

| | $S_1$ (eV) | $T_1$[a] (eV) | $\Phi_F$ |
|---|---|---|---|
| PPD | 3.99 | 2.82 | 0.85 |
| TP | 3.95 | 2.62 | 0.98 |
| 2PI | 3.71 | 2.22 | 0.78 |
| PPO | 3.67 | 2.40 | 0.81 |
| PPF | 3.59 | 2.28 | 0.86 |
| TIPS-naph | 3.53 | 2.12 | 0.76 |

[a]Literature values, for references see Table 2.1.

Table 2.1 are displayed alongside the singlet state energies in Table 4.2. One factor to consider is the thermodynamic driving force for TTA, which can be expressed as $[2 \times E(T_1) - E(S_1)]$. In this project, the TTA driving force is very large for all annihilators, with the smallest being 0.7 eV for 2PI and TIPS-naph. Hence, the TTA efficiency is not expected to significantly be affected by the variations of TTA driving force within the annihilators included in this project.

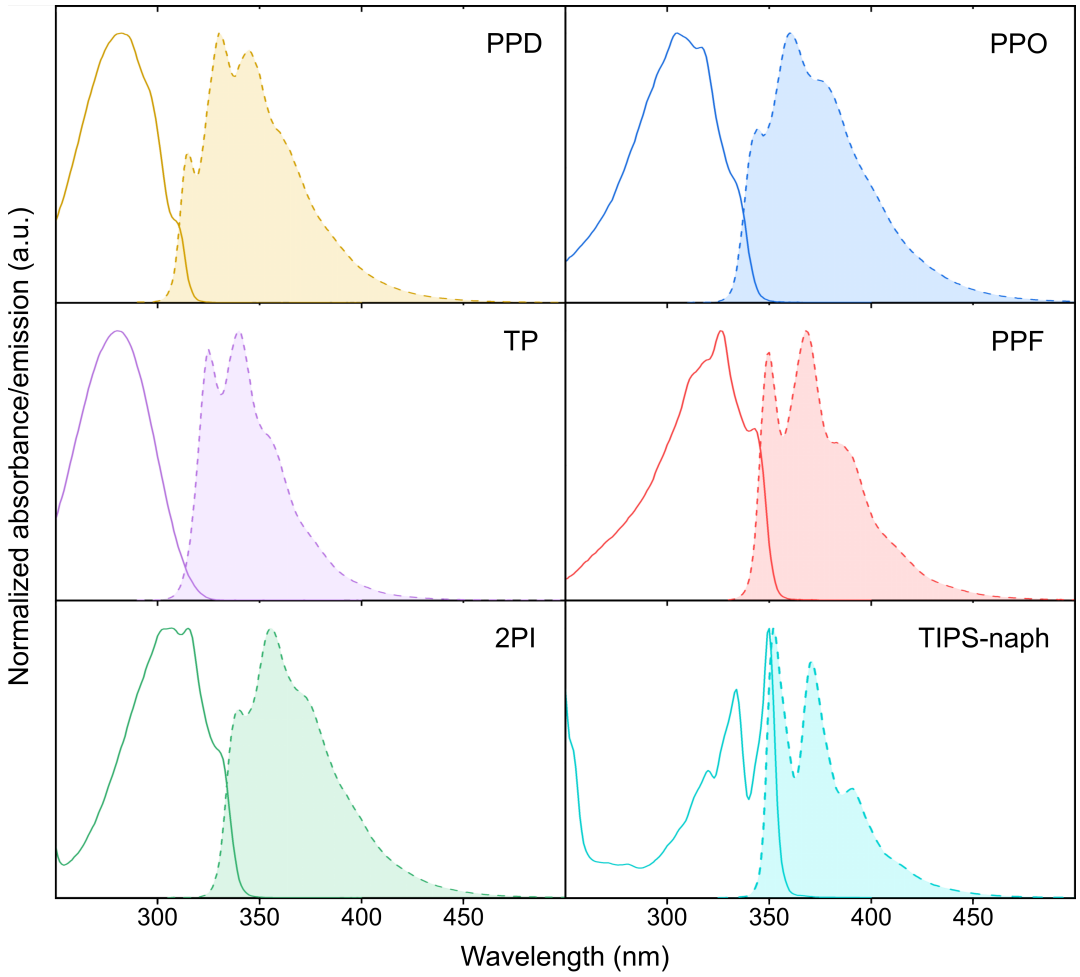



**Figure 4.2:** Normalized absorption (solid) and emission (dashed) spectra of the annihilators measured at room temperature in THF.

Another interesting aspect to compare is the difference in $E(T_1)$ between sensitizer and annihilator, which describes the driving force for TET. The triplet energy of 4CzBN was 2.7 eV, which results in endothermic TET from 4CzBN to PPD, and exothermic driving forces for the other annihilators, ranging up to 0.6 eV for TIPS-naph. The TET rate is expected to be slower when the driving force is small, thus resulting in less efficient TET. However, this is discussed further below together with the results of the TET measurements.

Something with a more direct effect on the UC efficiency is the fluorescence quantum yield of the UV emitters, which are also presented in Table 4.2. Although none of the annihilators have quantum yields reaching unity, they are all quite high.

## 4.3 Upconversion measurements

For all six annihilators, UC emission was detected when paired with the sensitizer 4CzBN, but as intended, to different extents. As the aim of this project was to understand why this was the case, several UC characteristics were determined, beyond measuring the UC quantum yields. The results from the measurements are presented and discussed separately below, but are all summarized in Table 4.3.

**Table 4.3:** Measured values of UC quantum yields and parameters important for TTA-UC systems.

| | $\Phi_{UC,g}$ | $\Phi_{UC}$ | $k_{TET}$ ($\times 10^9$ $M^{-1}$ $s^{-1}$) | $\tau_T$ (ms) | $I_{th}$ (mW $cm^{-2}$) | $\beta_{max}$ |
|---|---|---|---|---|---|---|
| PPD | 0.014 | 0.012 | 0.14 | 0.050 | - | 0.70 |
| TP | 0.045 | 0.034 | 0.29 | 0.086 | 3300 | 0.66 |
| 2PI | 0.017 | 0.014 | 2.2 | 0.22 | 3700 | 0.92 |
| PPO | 0.114 | 0.099 | 1.4 | 0.24 | 1300 | 0.90 |
| PPF | 0.110 | 0.085 | 2.0 | 0.19 | 550 | 0.86 |
| TIPS-naph | 0.038 | 0.026 | - | 0.60 | 90 | 0.91 |

### 4.3.1 TET rates and efficiencies

The TET efficiency ($\Phi_{TET}$) was estimated by probing the difference in delayed component lifetime at different annihilator concentrations according to Equation 2.15. The resulting Stern-Volmer plot is shown in Figure 4.3. Steeper lines correspond to more efficient TET. The TET rates ($k_{TET}$) were calculated from the slopes and are

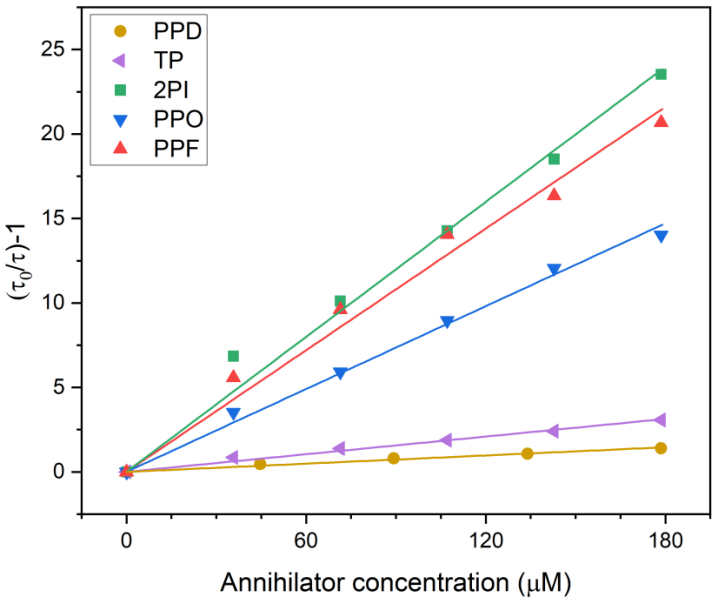



**Figure 4.3:** Stern-Volmer plots showing the change of 4CzBN delayed component lifetime upon addition of different concentrations of annihilator.

presented in Table 4.3. As expected from the discussion of the TET driving force, $k_{TET}$ is smallest for PPD and then TP. The TET rates for PPO, PPF and 2PI are in the expected order from the triplet excited state energies, too, but their differences are small, all three rates are around $2 \times 10^9$ $M^{-1}$ $s^{-1}$. This could be regarded as a result of the driving force reaching a "high enough" level for the TET efficiency to instead primarily depend on the diffusion rate.

Unfortunately, the TET rate from 4CzBN to TIPS-naph was not measured. However, due to the low triplet energy of TIPS-naph, and thus the large TET driving force, it can be assumed that the rate was sufficiently large to obtain efficient TET.

The annihilator concentration of the UC samples, 10 mM, was chosen in order to give efficient TET for all annihilators. This concentration gives a $\Phi_{TET}$ as high as 0.89 even for the endothermic TET from 4CzBN to PPD (Note that the ISC event is included in the herein used definition of $\Phi_{TET}$, and thus the highest possible value of $\Phi_{TET} = \Phi_{ISC} = 0.90$). Due to the high annihilator concentration in the UC samples, the differences in TET rates are not expected to have a considerable effect on the overall UC efficiency.

### 4.3.2 Triplet lifetimes

Although the annihilator triplet lifetime ($\tau_T$) is not included in the expression for the upconversion quantum yield (Equation 2.10), it is still one of the main parameters dictating the performance of TTA-UC in solutions. Since the TTA event requires triplet excited annihilators to encounter, a longer triplet lifetime gives more time for the molecules to diffuse and thus, a higher probability of two annihilators encountering before decaying through other channels.

The triplet excited state lifetimes of the annihilators were determined by probing the lifetime of UC emission at different excitation intensities, and then globally fit these to Equation 3.5. The fitting for PPO is shown in Figure 4.4 as an example, while the fittings for the other annihilators can be seen in Appendix B. The resulting annihilator triplet lifetimes are presented in Table 4.3. The shortest $\tau_T$ was found for PPD and TP, 0.050 and 0.086 ms, respectively. The longest triplet lifetime was approximately ten times greater, 0.60 ms for TIPS-naph.

### 4.3.3 $\beta$ values and TTA efficiency

One more parameter that originates from the triplet lifetimes measurements is presented in Table 4.3, the maximal values of the dimensionless parameter $\beta$. Since $\beta$ describes the fraction of triplets decaying through TTA, it is directly connected to the TTA efficiency. If the triplet lifetime measurements are done at identical experimental conditions as the UC measurements, $\Phi_{TTA} = \beta/2$. Unfortunately, this was not the case for the lifetime measurement presented here, which used a different excitation source compared to the UC measurements. However, even if $\beta_{max}$ cannot be used to calculate $\Phi_{TTA}$, it can still give an indication of the TTA efficiency. $\beta_{max}$ is approximately 0.9 for all annihilators but PPD and TP, which has a $\beta_{max}$ of about 0.7. This suggests that the TTA is less efficient for PPD and TP, a notion that also coincides with them having comparatively short triplet lifetimes.

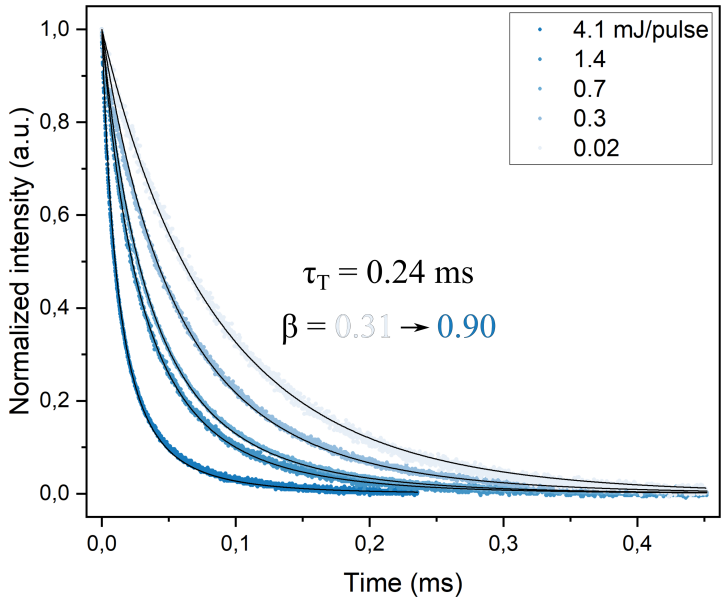



**Figure 4.4:** Determination of PPO triplet lifetime. Normalized time-domain measurement of UC emission from 100 $\mu$M 4CzBN / 10 mM PPO at different excitation intensities, globally fitted according to Equation 3.5.

### 4.3.4 Intensity thresholds

The last determined UC characteristic is the intensity threshold. Figure 4.5 shows the intensity series for TIPS-naph, which with $I_{th}$ = 90 mW/cm$^2$ was the annihilator with the lowest intensity threshold. For the other annihilators, the intensity thresholds range from about a half to a few W/cm$^2$, and their respective values can be seen in Table 4.3. Due to a too weak UC signal, the intensity threshold for PPD could not be determined.

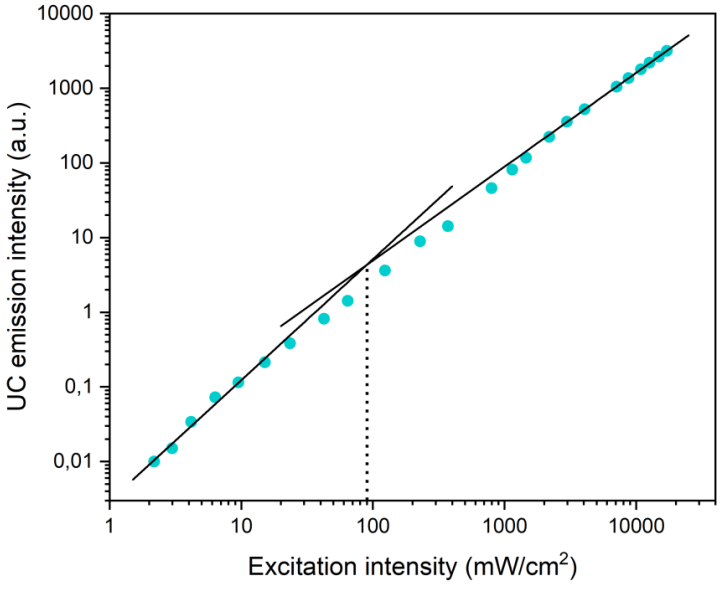



**Figure 4.5:** Determination of intensity threshold for TIPS-naph.

As the goal is to be able to use the sun as the excitation source in the future, the intensity thresholds observed in this project are all too high. However, the intensity threshold is directly dependent on the concentration of the sensitizer (see Equation 2.12), and will decrease with increasing concentration. Though this in turn would increase the reabsorption of UC photons, that could be alleviated by changing the sample properties, like for example shorten the distance the UC photons travel through the solution.

### 4.3.5 Upconversion quantum yields

As already mentioned, all annihilators realized TTA-UC when coupled with 4CzBN. Their generated and observed UC quantum yields were evaluated from samples of 25 $\mu$M 4CzBN and 10 mM annihilator, and according to the fitting procedure described in the Methods chapter (Section 3.4.2). Measured UC spectra for all annihilators, and their respective fittings, can be found in Appendix B (Figure B.3), while the determined quantum yields are given in Table 4.3 and presented as a bar chart in Figure 4.6. Though $\Phi_{UC,g}$ accounts for the strong reabsorption of high-energy UC photons through the fitting procedure, the results are likely somewhat underestimated, as no additional corrections were made, even if the absorbance at the fitting wavelengths was not negligible. All yields were determined based on the results of at least three individual samples, and the standard deviations are displayed as error bars in Figure 4.6.

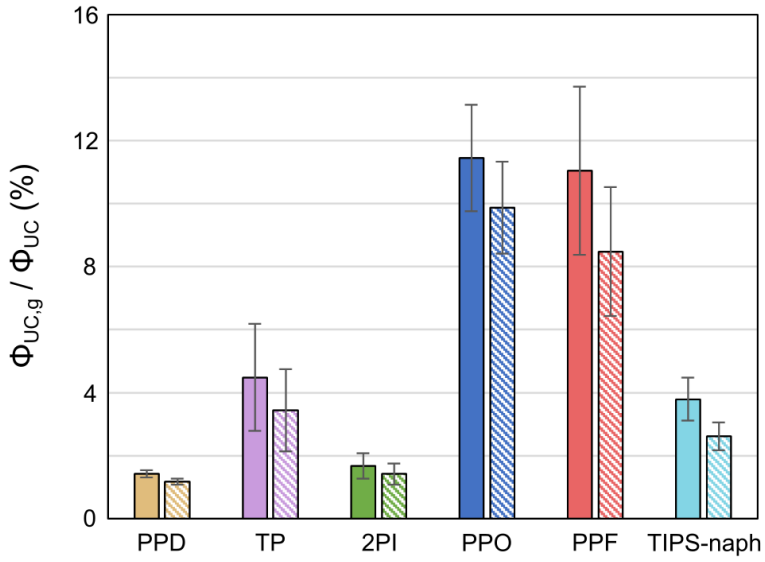



**Figure 4.6:** Quantum yields of UC photons generated (solid) and UC photons observed (striped). The error bars indicate the standard deviation.

The highest quantum yields were achieved for PPO and PPF, with $\Phi_{UC,g}$ of 0.114 and 0.110, respectively. Although the aim of this project was not to attain record-high quantum yields, it is worth mentioning that these values are exceptionally good, as the 10 % limit only has been surpassed for vis-to-UV upconversion in three previous studies.[10, 11, 12] The quantum yields of the two deeper UV-emitting

annihilators PPD and TP (0.014 and 0.045, respectively) are also improvements compared to previous studies.[11, 30]

With an internal UC quantum yield of 0.038, TIPS-naph did not approach its anticipated efficiency, as it has previously been utilized in two different systems reaching quantum yields just above 10 %.[10, 12] The UC samples with TIPS-naph had somewhat distorted UC emission spectra, and in addition strangely shaped absorption spectra. This created suspicions that the sample may be contaminated by another fluorophore. At the conclusion of this Master's thesis, the project continued by Olesund et al.[27] and it turned out that this was the case. Evaluated at the same experimental conditions as the UC samples within this thesis, they attained a new $\Phi_{UC,g} = 0.141$ for samples with 1 mM recrystallized TIPS-naph.

2PI is one of the annihilators which were new for the application of TTA-UC and had a generated UC quantum yield of 0.017. With $\Phi_F$, $k_{TET}$, $\tau_T$ and $\beta_{max}$ values all quite similar to those of both PPO and PPF, the quantum yield of 2PI can appear as surprisingly low. But like for TIPS-naph, an unexpected behavior was observed for 2PI during the UC measurements, which will be discussed further below. However, due to this special behavior, 2PI will be disregarded when further discussing the quantum yields.

As already mentioned, it is assumed that $k_{TET}$ does not have a strong impact over the UC quantum yields due to the high annihilator concentration. The intensity threshold is an important parameter due to the long-term goal of using the sun as excitation source, but since the UC samples were examined at a laser fluence of 18 W/cm$^2$, the different values of the intensity thresholds are assumed to not affect the UC quantum yields observed in this project. Since the values of $\beta_{max}$ were determined with a different experimental setup, no great significance can be given to them when discussing the UC quantum yields. However, it can be mentioned that PPD and TP, which had slightly lower $\beta_{max}$ than the other annihilators, also was the ones with lower UC quantum yields.

The remaining parameter is the lifetime of the first triplet excited state of the annihilator. PPD had the smallest UC quantum yield and the shortest $\tau_T$ (50 $\mu$s), while the more efficient of the two deeper UV emitters, TP, had a longer triplet lifetime (86 $\mu$s). This was the second shortest $\tau_T$, and furthermore, TP had the second lowest UC quantum yield. PPO and PPF had similar values for both $\Phi_{UC,g}$ and $\tau_T$, although slightly higher/longer for PPO. The highest UC quantum yield was attained for the recrystallized TIPS-naph ($\Phi_{UC,g} = 0.141$), and TIPS-naph had the longest triplet lifetime, almost three times as long as for any other annihilator. To conclude, it can easily be stated that the triplet lifetime of the annihilator is a very important parameter for the efficiency of TTA-UC systems.

#### 4.3.5.1 System instability and solvents

The variation of the determined quantum yields was generally large, which were the reason why some annihilators was analyzed by more than three individual samples. The main reason for the large uncertainties is probably the instability of the UC emission signal. Although to different degrees, it was noticed that the intensity of the emission signal for the UC samples decreased over time (examples are shown in Figure 4.7A and B.4). Therefore, the samples used for the determination of the

UC quantum yields were studied by measuring the UC emission over time at a fixed wavelength. More particularly at the wavelength which gave the maximal observed UC emission for the current annihilator, which ranged from 340 nm for TP to 373 nm for TIPS-naph.

If not otherwise mentioned, all measurements in this study were conducted in tetrahydrofuran (THF) as the solvent. THF was chosen primarily since it readily dissolved all sample compounds, but another advantage is that the absorption of THF does not interfere with the absorption of the annihilators at shorter wavelengths. However, at the end of this thesis project it was speculated whether the solvent affected the stability of the system. The solubility in hexane and toluene were tested, and the latter managed to dissolve the sample compounds, although not as easily as THF. Two UC samples in toluene was measured and compared to similar samples in THF (Figure 4.7). Although the UC emission signal still decreased over time, the stability of the signal was significantly improved for the samples in toluene. Therefore, toluene was used as the main solvent when the project continued after the completion of the measurements in this thesis.[27]

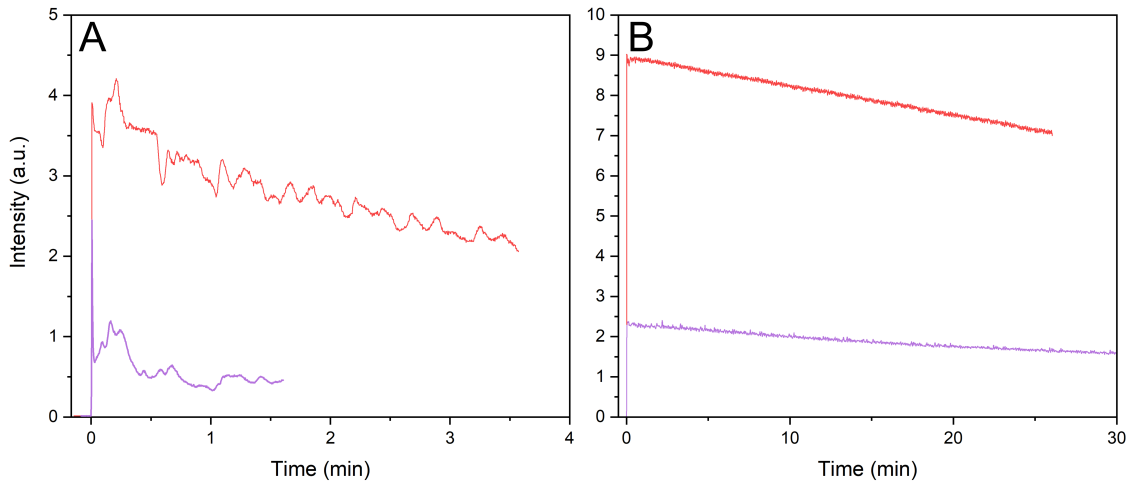



**Figure 4.7:** The decrease of UC emission intensity over time for samples of 25 $\mu$M 4CzBN and 10mM PPF (red lines) or TP (purple lines) in (A) THF, and (B) toluene.

#### 4.3.5.2 Scattering and 2PI solubility

At first, light scattering was detected in the absorption spectrum of the UC sample for 2PI, from noticing that the absorption slowly increased by shorter wavelengths before the actual absorption onset at about 430 nm (Figure 4.8A). Then, it was observed that the UC emission signal greatly increased over time (Figure 4.8B). In addition, after about 80 minutes of exposure to 405 nm excitation, the light scattering noticeable in the absorption spectrum had significantly decreased. Since scattering commonly occurs from solutions containing larger molecules or particles, it is supposed that the sample with 10 mM 2PI includes undissolved micro crystals of the annihilator. The sample gradually dissolved, either only by time, or by the impact of the excitation light, which is why the scattering had decreased after

the UC measurement. High annihilator concentrations promote diffusion-controlled processes like TET and TTA, hence the UC efficiency improved over time as the concentration of dissolved 2PI molecules increased.

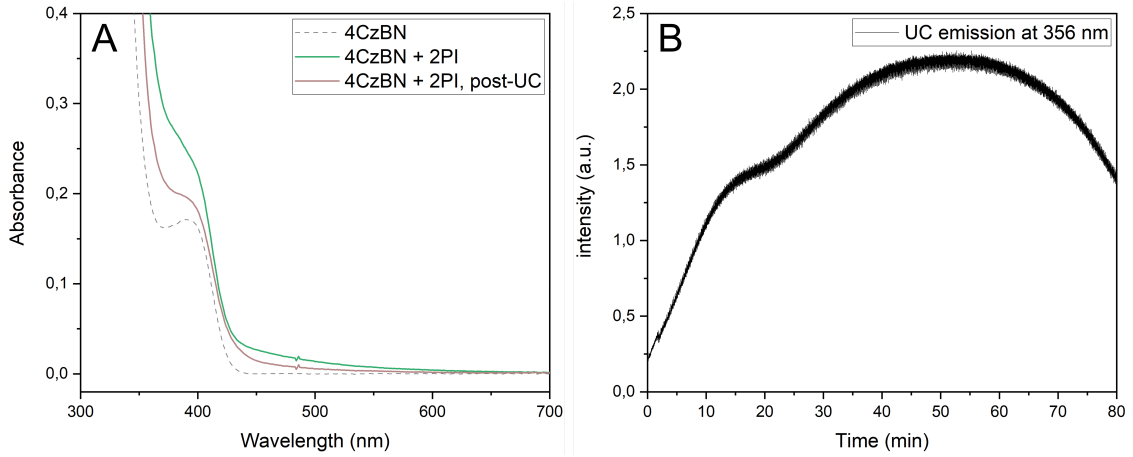



**Figure 4.8:** (A) Absorption spectra of 4CzBN (dashed line), and 4CzBN + 10 mM 2PI measured before (green) and after (brown) 80 minutes of 405 nm laser irradiation. (B) Time development of UC emission signal for 2PI measured at 356 nm.

# 5
# Conclusion

In this project, the efficiencies of TTA-UC systems using six different UV emitting molecules have been analyzed. Four of the UV emitters have been utilized as annihilators previously, while two were new in this application. Vis-to-UV upconversion was realized for all annihilators when coupled with the purely organic, TADF compound 4CzBN as sensitizer. Internal quantum yields ranging from 1.4 % for PPD to 11 % for PPO and PPF were attained, which are all excellent results when compared to previous studies.

Unfortunately, the variations of the results were generally large, as the UC emission was very unstable and quickly degenerating. A few initial measurements indicated that the solvent had a large effect on the system stability. Although the UV emission still degraded over time, the stability greatly improved when changing from THF to toluene as the solvent.

The aim of this project was to increase the knowledge about annihilators and their impact on the UC efficiency, and hence, several UC characteristics were evaluated. The results show that the most important parameter affecting the quantum yield was the annihilator triplet excited state lifetime. Using the blue-emitting 4CzBN as sensitizer makes the apparent anti-Stokes shifts relatively small, and for the future, it would be beneficial if the excitation wavelength could be extended further into the visible region.

To continue developing highly efficient vis-to-UV upconversion systems, new compounds must be discovered both for the application of annihilators and as sensitizers. Primarily, long triplet lifetimes are required to achieve systems with high quantum yields. Controlling and changing the energy levels of both their singlet and triplet states can help increase the apparent anti-Stokes shift, and thus, increase the energy gain of the process. Additionally, it is vital to solve the issue regarding the degradation of the system. Nevertheless, the results presented herein provide an important step forward by demonstrating several TTA-UC systems with high quantum yields, and by emphasizing the importance of long annihilator triplet lifetimes.

# Bibliography


[1] E. Kabir, P. Kumar, S. Kumar, A. A. Adelodun, and K. H. Kim, "Solar energy: Potential and future prospects," 2 2018.

[2] W. Chen, W. Shen, H. Wang, F. Liu, L. Duan, X. Xu, D. Zhu, M. Qiu, E. Wang, and R. Yang, "Enhanced efficiency of polymer solar cells by improving molecular aggregation and broadening the absorption spectra," *Dyes and Pigments*, vol. 166, pp. 42–48, 7 2019.

[3] N. Yao, J. Huang, K. Fu, X. Deng, M. Ding, M. Shao, and X. Xu, "Enhanced light harvesting of dye-sensitized solar cells with up/down conversion materials," *Electrochimica Acta*, vol. 154, pp. 273–277, 2 2015.

[4] T. N. Singh-Rachford and F. N. Castellano, "Photon upconversion based on sensitized triplet-triplet annihilation," 11 2010.

[5] E. M. Gholizadeh, S. K. Prasad, Z. L. Teh, T. Ishwara, S. Norman, A. J. Petty, J. H. Cole, S. Cheong, R. D. Tilley, J. E. Anthony, S. Huang, and T. W. Schmidt, "Photochemical upconversion of near-infrared light from below the silicon bandgap," *Nature Photonics*, vol. 14, pp. 585–590, 9 2020.

[6] B. Pfund, D. M. Steffen, M. R. Schreier, M. S. Bertrams, C. Ye, K. Börjesson, O. S. Wenger, and C. Kerzig, "UV Light Generation and Challenging Photoreactions Enabled by Upconversion in Water," *Journal of the American Chemical Society*, vol. 142, pp. 10468–10476, 6 2020.

[7] S. Sharma and S. K. Ghoshal, "Hydrogen the future transportation fuel: From production to applications," 2015.

[8] H. Kato, K. Asakura, and A. Kudo, "Highly efficient water splitting into H2 and O2 over lanthanum-doped NaTaO3 photocatalysts with high crystallinity and surface nanostructure," *Journal of the American Chemical Society*, vol. 125, pp. 3082–3089, 3 2003.

[9] T. N. Singh-Rachford and F. N. Castellano, "Low power visible-to-UV upconversion," *Journal of Physical Chemistry A*, vol. 113, pp. 5912–5917, 5 2009.

[10] N. Harada, Y. Sasaki, M. Hosoyamada, N. Kimizuka, and N. Yanai, "Discovery of Key TIPS-Naphthalene for Efficient Visible-to-UV Photon Upconversion under Sunlight and Room Light**," *Angewandte Chemie - International Edition*, vol. 60, pp. 142–147, 1 2021.

[11] L. Hou, A. Olesund, S. Thurakkal, X. Zhang, and B. Albinsson, "Efficient Visible-to-UV Photon Upconversion Systems Based on CdS Nanocrystals Modified with Triplet Energy Mediators," *Advanced Functional Materials*, vol. 31, 11 2021.

[12] M. Uji, N. Harada, N. Kimizuka, M. Saigo, K. Miyata, K. Onda, and N. Yanai, "Heavy metal-free visible-to-UV photon upconversion with over 20% efficiency

sensitized by a ketocoumarin derivative," *Journal of Materials Chemistry C*, vol. 10, no. 12, pp. 4558–4562, 2022.

[13] W. Sun, A. Ronchi, T. Zhao, J. Han, A. Monguzzi, and P. Duan, "Highly efficient photon upconversion based on triplet-triplet annihilation from bichromophoric annihilators," *Journal of Materials Chemistry C*, vol. 9, pp. 14201–14208, 10 2021.

[14] J. R. Lakowicz, *Principles of Fluorescence Spectroscopy*. Springer, 3rd ed., 2006.

[15] Y. Zhou, F. N. Castellano, T. W. Schmidt, and K. Hanson, "On the Quantum Yield of Photon Upconversion via Triplet-Triplet Annihilation," 7 2020.

[16] Y. Y. Cheng, B. Fückel, T. Khoury, R. G. Clady, M. J. Tayebjee, N. J. Ekins-Daukes, M. J. Crossley, and T. W. Schmidt, "Kinetic analysis of photochemical upconversion by triplet-triplet annihilation: Beyond any spin statistical limit," *Journal of Physical Chemistry Letters*, vol. 1, pp. 1795–1799, 6 2010.

[17] D. Y. Kondakov, T. D. Pawlik, T. K. Hatwar, and J. P. Spindler, "Triplet annihilation exceeding spin statistical limit in highly efficient fluorescent organic light-emitting diodes," *Journal of Applied Physics*, vol. 106, no. 12, 2009.

[18] D. G. Bossanyi, Y. Sasaki, S. Wang, D. Chekulaev, N. Kimizuka, N. Yanai, and J. Clark, "Spin Statistics for Triplet–Triplet Annihilation Upconversion: Exchange Coupling, Intermolecular Orientation, and Reverse Intersystem Crossing," *JACS Au*, vol. 1, pp. 2188–2201, 12 2021.

[19] A. Monguzzi, J. Mézyk, F. Scotognella, R. Tubino, and F. Meinardi, "Upconversion-induced fluorescence in multicomponent systems: Steady-state excitation power threshold," *Physical Review B - Condensed Matter and Materials Physics*, vol. 78, 11 2008.

[20] T. C. Wu, D. N. Congreve, and M. A. Baldo, "Solid state photon upconversion utilizing thermally activated delayed fluorescence molecules as triplet sensitizer," *Applied Physics Letters*, vol. 107, 7 2015.

[21] N. Yanai, M. Kozue, S. Amemori, R. Kabe, C. Adachi, and N. Kimizuka, "Increased vis-to-UV upconversion performance by energy level matching between a TADF donor and high triplet energy acceptors," *Journal of Materials Chemistry C*, vol. 4, no. 27, pp. 6447–6451, 2016.

[22] Y. Wei, K. Pan, X. Cao, Y. Li, X. Zhou, C. Yang, Y. Wei, K. Pan, X. Cao, C. Yang, Y. Li, and X. Zhou, "Multiple Resonance TADF Sensitizers Enable Green-to-Ultraviolet Photon Upconversion: Application in Photochemical Transformations," tech. rep., 2021.

[23] W. Chen, F. Song, S. Tang, G. Hong, Y. Wu, and X. Peng, "Red-to-blue photon up-conversion with high efficiency based on a TADF fluorescein derivative," *Chemical Communications*, vol. 55, no. 30, pp. 4375–4378, 2019.

[24] H. L. Lee, M. S. Lee, H. Park, W. S. Han, and J. H. Kim, "Visible-to-UV triplet-triplet annihilation upconversion from a thermally activated delayed fluorescence/pyrene pair in an air-saturated solution," *Korean Journal of Chemical Engineering*, vol. 36, pp. 1791–1798, 11 2019.

[25] F. B. Dias, T. J. Penfold, and A. P. Monkman, "Photophysics of thermally activated delayed fluorescence molecules," 3 2017.

[26] D. Zhang, M. Cai, Y. Zhang, D. Zhang, and L. Duan, "Sterically shielded blue thermally activated delayed fluorescence emitters with improved efficiency and stability," *Materials Horizons*, vol. 3, pp. 145–151, 3 2016.

[27] A. Olesund, J. Johnsson, F. Edhborg, S. Ghasemi, K. Moth-Poulsen, and B. Albinsson, "Approaching the Spin-Statistical Limit in Visible-to-Ultraviolet Photon Upconversion," *Journal of the American Chemical Society*, vol. 144, pp. 3706–3716, 3 2022.

[28] V. Gray, P. Xia, Z. Huang, E. Moses, A. Fast, D. A. Fishman, V. I. Vullev, M. Abrahamsson, K. Moth-Poulsen, and M. Lee Tang, "CdS/ZnS core-shell nanocrystal photosensitizers for visible to UV upconversion," *Chemical Science*, vol. 8, no. 8, pp. 5488–5496, 2017.

[29] P. B. Merkel and J. P. Dinnocenzo, "Low-power green-to-blue and blue-to-UV upconversion in rigid polymer films," *Journal of Luminescence*, vol. 129, pp. 303–306, 3 2009.

[30] B. Yurash, A. Dixon, C. Espinoza, A. Mikhailovsky, S. Chae, H. Nakanotani, C. Adachi, and T. Q. Nguyen, "Efficiency of Thermally Activated Delayed Fluorescence Sensitized Triplet Upconversion Doubled in Three-Component System," *Advanced Materials*, vol. 34, 2 2022.

[31] C. Rulliere and P. C. Roberge, "Photophysics of aryl substituted 1,3,4-oxadiazoles: The triplet state of 2.5-diphenyl-1,3,4-oxadiazole," *Chemical Physics Letters*, vol. 97, pp. 247–252, 5 1983.

[32] P. B. Merkel and J. P. Dinnocenzo, "Thermodynamic energies of donor and acceptor triplet states," *Journal of Photochemistry and Photobiology A: Chemistry*, vol. 193, pp. 110–121, 1 2008.

[33] I. B. Berlman, *Handbook of Fluorescence Spectra of Aromatic Molecules*. New York and London: Academic Press, 2nd ed., 1971.

[34] C. Würth, M. Grabolle, J. Pauli, M. Spieles, and U. Resch-Genger, "Relative and absolute determination of fluorescence quantum yields of transparent samples," *Nature Protocols*, vol. 8, no. 8, pp. 1535–1550, 2013.

[35] F. Edhborg, H. Bildirir, P. Bharmoria, K. Moth-Poulsen, and B. Albinsson, "Intramolecular Triplet-Triplet Annihilation Photon Upconversion in Diffusionally Restricted Anthracene Polymer," *Journal of Physical Chemistry B*, vol. 125, pp. 6255–6263, 6 2021.

[36] A. Olesund, V. Gray, J. Mårtensson, and B. Albinsson, "Diphenylanthracene Dimers for Triplet-Triplet Annihilation Photon Upconversion: Mechanistic Insights for Intramolecular Pathways and the Importance of Molecular Geometry," *Journal of the American Chemical Society*, vol. 143, pp. 5745–5754, 4 2021.

# A

# Appendix 1: Derivations

## A.1 TET efficiency for TADF sensitizers

The original expression for $\Phi_{TET}$ from section 2.2.1 is

$$\Phi_{TET} = 1 - \frac{F_{DA}}{F_D} = 1 - \frac{\tau_{DA}}{\tau_D} = 1 - \frac{1}{1 + k_{TET}\tau_D[A]} \tag{2.9}$$

In section 2.3.1 it is described that for TADF sensitizers, $\Phi_{ISC}$ should be included in the expression for $\Phi_{TET}$. It is also explained why the approximate method used in this project is evaluating the change in lifetime of the delayed component upon addition of annihilator. A new expression for $\Phi_{TET}$ is thus

$$\Phi_{TET} = \Phi_{ISC}\left(1 - \frac{\tau_{DF}}{\tau_{DF,0}}\right) = \Phi_{ISC}\left(1 - \frac{1}{1 + k_{TET}\tau_{DF,0}[A]}\right) \tag{A.1}$$

The expression within the parenthesis to the right may be simplified according to Equation A.2 below. As the lifetime of the delayed component is governed by the lifetime of the triplet excited state, $\tau_{DF,0} = \tau_T$. The relationship between lifetime and rate is also used, $\tau_{DF,0} = \tau_T = 1/k_T$. Note that here, $k_T = k_{ph} + k_{nr,T}$, as opposed to $k_T$ in Equation 2.14 where it also contains the term $k_{TET}[Q]$. The reason is that for this expression, $k_T$ denotes the decay rate of the triplet state for an unquenched sensitizer and hence, the TET pathway is not available.

$$1 - \frac{1}{1 + k_{TET}\tau_{DF,0}[A]} = 1 - \frac{1}{1 + k_{TET}(1/k_T)[A]} = 1 - \frac{k_T}{k_T + k_{TET}[A]} =$$

$$= \frac{k_T + k_{TET}[A]}{k_T + k_{TET}[A]} - \frac{k_T}{k_T + k_{TET}[A]} = \frac{k_{TET}[A]}{k_T + k_{TET}[A]} \tag{A.2}$$

Subsequently, the simpler expression for $\Phi_{TET}$ can be created,

$$\Phi_{TET} = \Phi_{ISC}\frac{k_{TET}[A]}{k_T + k_{TET}[A]} \tag{2.16}$$

## A.2 Determination of TET rate

By combining Equations A.1 and 2.16 one can get

$$1 - \frac{\tau_{DF}}{\tau_{DF,0}} = \frac{k_{TET}[A]}{k_T + k_{TET}[A]} \tag{A.3}$$

which can further be simplified as

$$\frac{\tau_{DF}}{\tau_{DF,0}} = 1 - \frac{k_{TET}[A]}{k_T + k_{TET}[A]}$$

$$\frac{\tau_{DF}}{\tau_{DF,0}} = \frac{k_T + k_{TET}[A] - k_{TET}[A]}{k_T + k_{TET}[A]}$$

$$\frac{\tau_{DF}}{\tau_{DF,0}} = \frac{k_T}{k_T + k_{TET}[A]}$$

$$\frac{\tau_{DF,0}}{\tau_{DF}} = \frac{k_T + k_{TET}[A]}{k_T}$$

$$\frac{\tau_{DF,0}}{\tau_{DF}} = 1 + \frac{k_{TET}[A]}{k_T}$$

$$\frac{\tau_{DF,0}}{\tau_{DF}} - 1 = \frac{k_{TET}[A]}{k_T}$$

and at last, resulting in the expression used for the Stern-Volmer plots,

$$\frac{\tau_{DF,0}}{\tau_{DF}} - 1 = k_{TET}\,\tau_{DF,0}\,[A] \tag{2.15}$$

# B

# Appendix 2: Additional figures

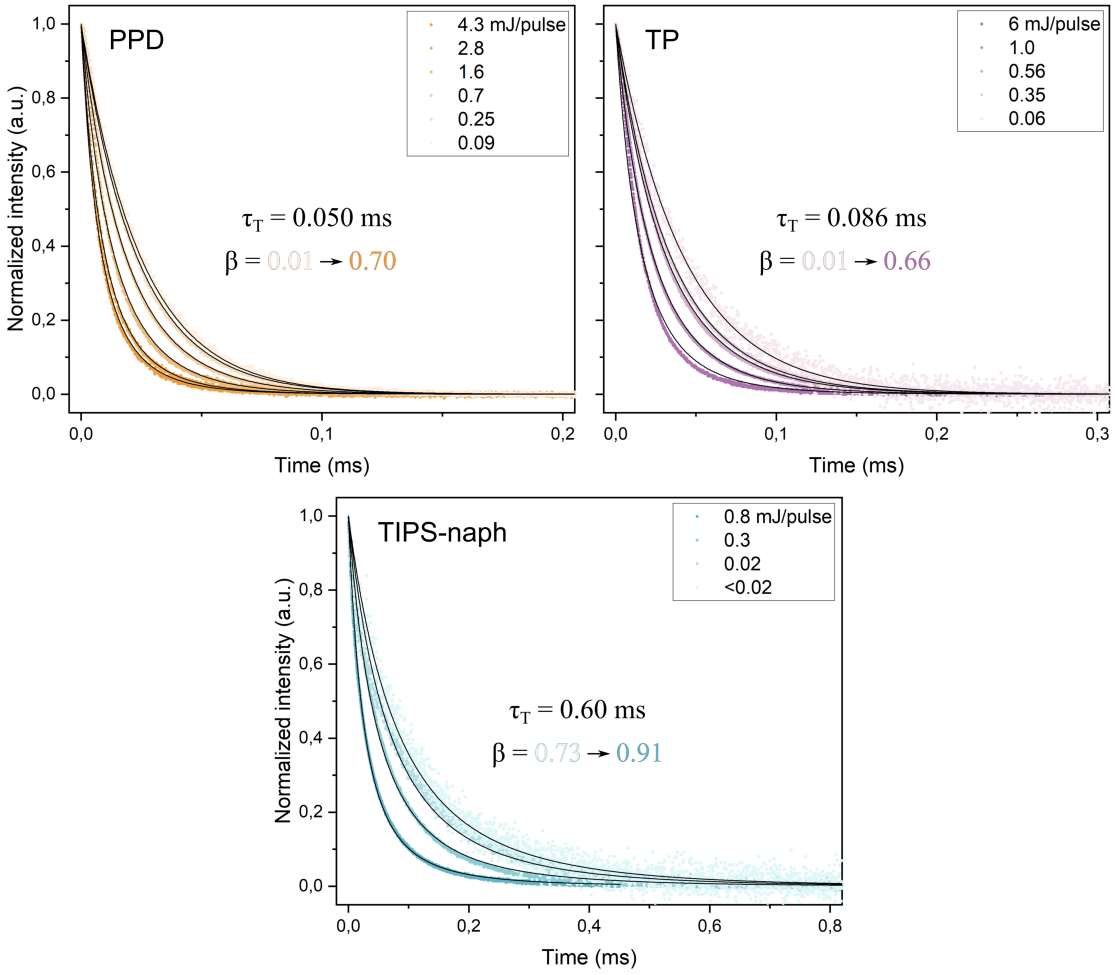



**Figure B.1:** Determination of PPD, TP and TIPS-naph triplet lifetimes. Global fitting of UC emission from 100 $\mu$M 4CzBN / 10 mM annihilator according to Equation 3.5.

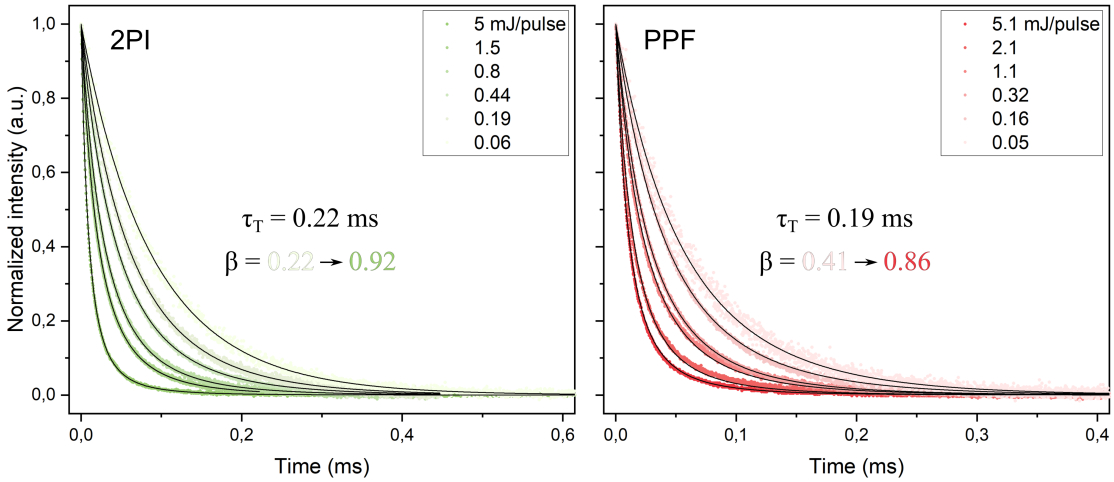



**Figure B.2:** Determination of 2PI and PPF triplet lifetimes. Global fitting of UC emission from 100 $\mu$M 4CzBN / 1 mM annihilator according to Equation 3.5.

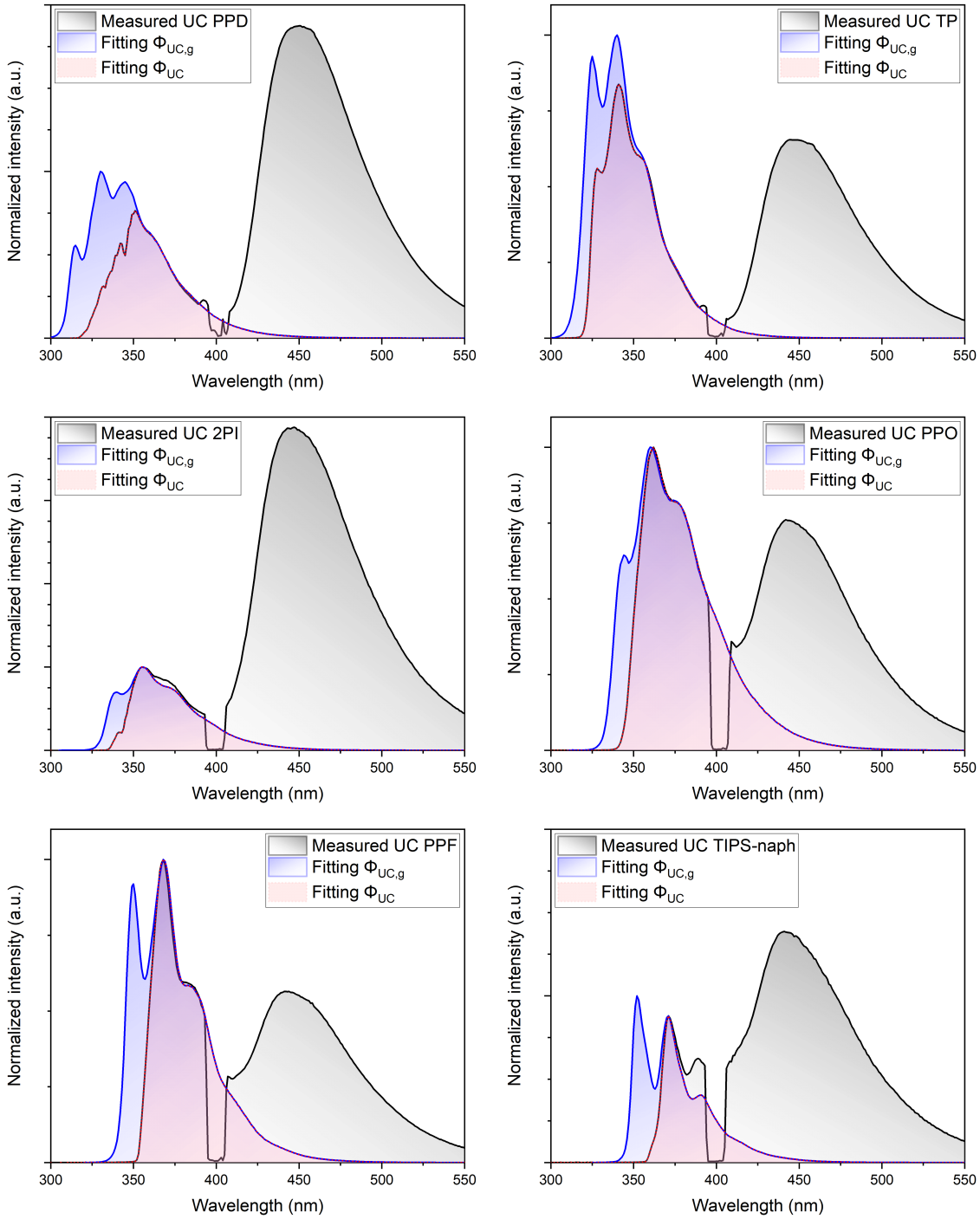



**Figure B.3:** Measured UC spectra (black) and fitted spectra to calculate $\Phi_{UC,g}$ (blue) and $\Phi_{UC,g}$ (red) for the different annihilators.

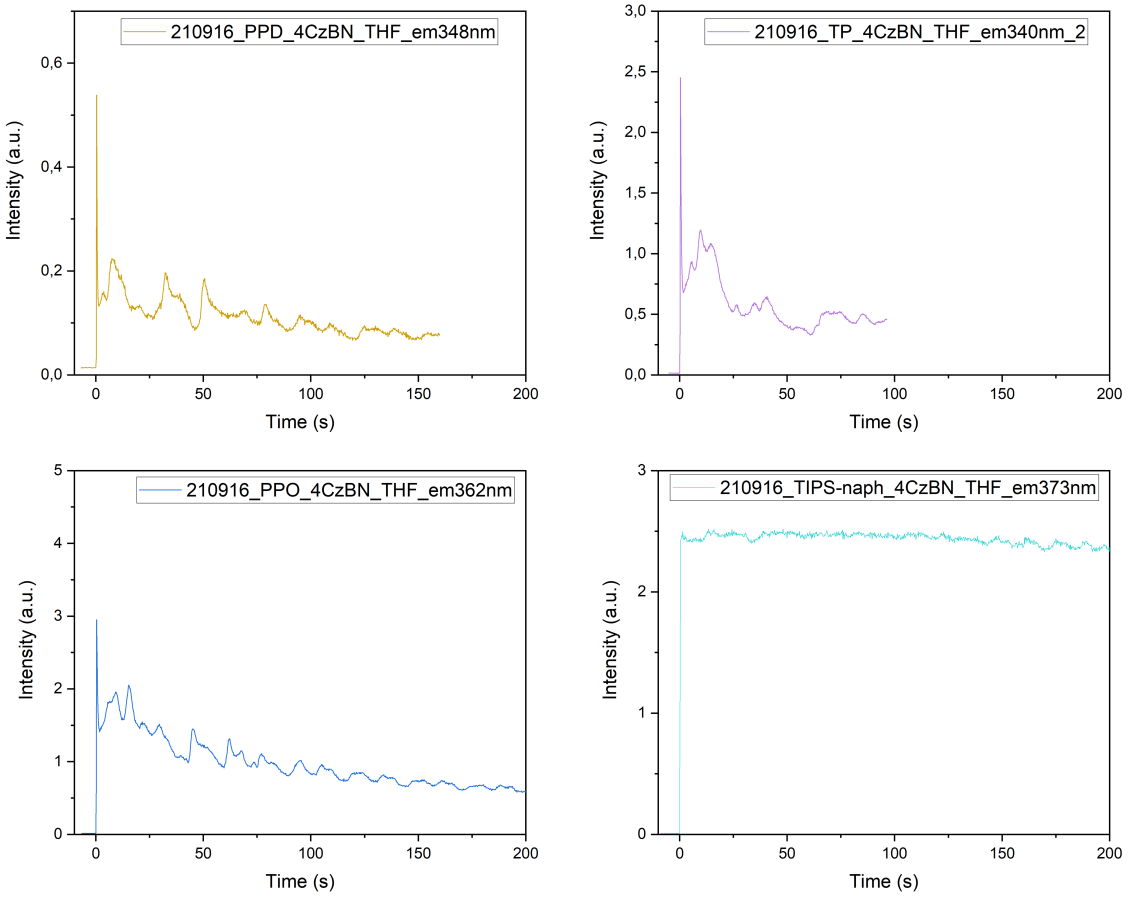



**Figure B.4:** Examples of how the UC emission intensity decrease over time.

**DEPARTMENT OF CHEMISTRY AND CHEMICAL ENGINEERING**
**CHALMERS UNIVERSITY OF TECHNOLOGY**
Gothenburg, Sweden
www.chalmers.se




CHALMERS
UNIVERSITY OF TECHNOLOGY